seiomm
Sociedad Española de Investigación Ósea y del Metabolismo Mineral

feiomm
Fundación Española de Investigación Ósea y del Metabolismo Mineral

Volume 12 · Number 2 · April-June 2020

Revista de Osteoporosis y Metabolismo Mineral

www.revistadeosteoporosisymetabolismomineral.com

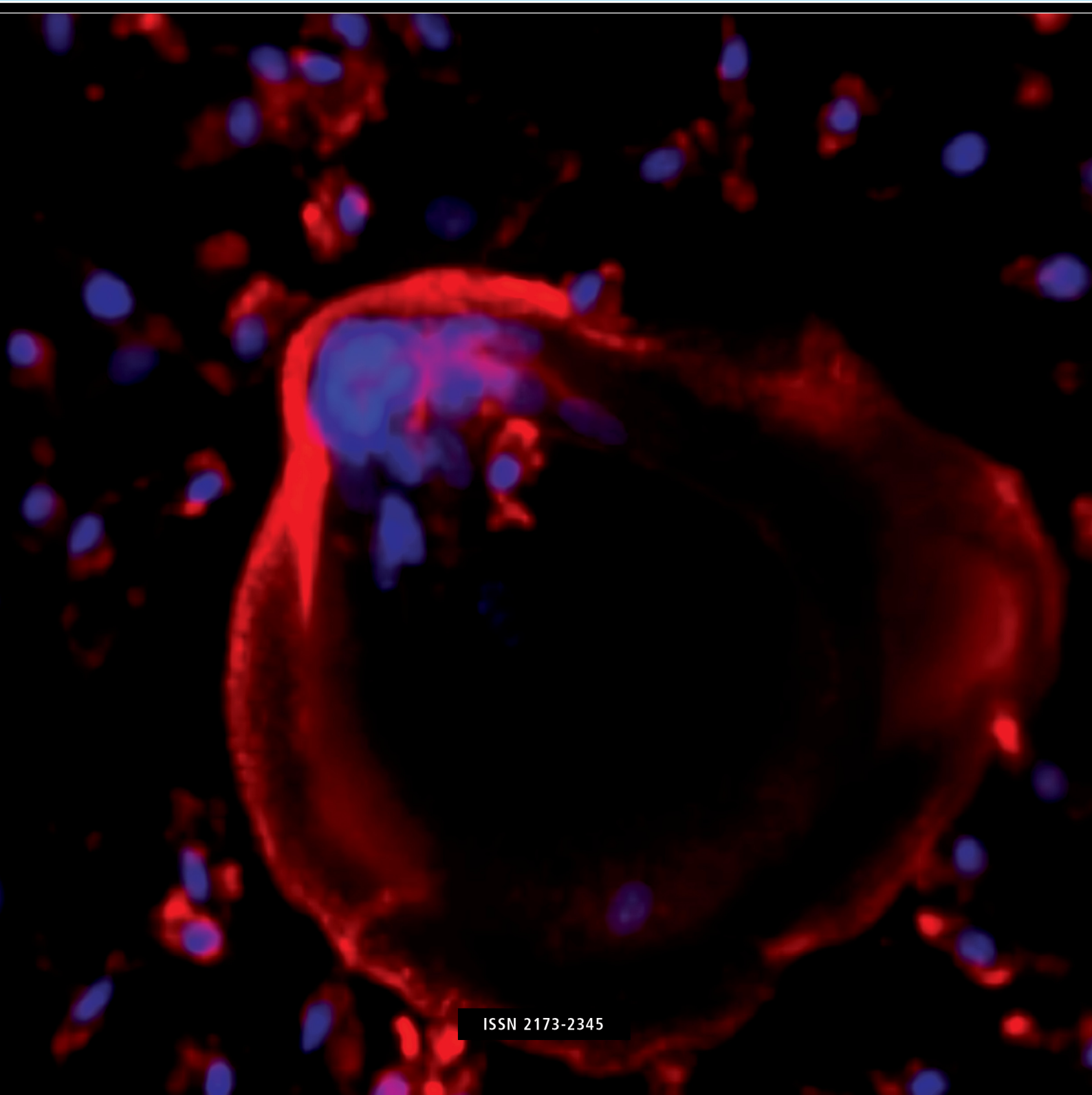

ISSN 2173-2345

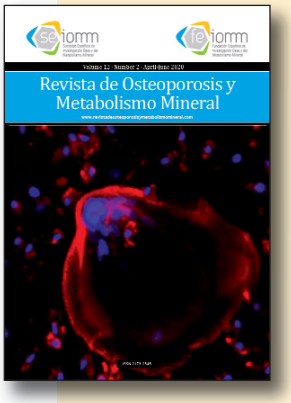

Our cover: Human osteoclast observed under a confocal microscope. The phalloidin stained actin ring (red) is observed; nuclei stained with DAPI (blue).
Author: Dra. Natalia Garcia Giralt, CIBERFES, Hospital del Mar Institute for Medical Research (IMIM), Barcelona (Spain)

Sociedad Española de Investigación Ósea y del Metabolismo Mineral (SEIOMM)

President
Manuel Naves Díaz

Vicepresident
Pilar Peris Bernal

Secretary
Minerva Rodríguez García

Treasurer
José Luis Pérez Castrillón

Members
Luis del Río Barquero
José Antonio Riancho Moral

Elect President
Guillermo Martínez Díaz-Guerra

Velázquez, 94 (1ª planta)
28006 Madrid (Spain)

Telf: +34-648 949 755

seiomm@seiomm.org

www.seiomm.org

Editing
Ibáñez & Plaza Asociados, S. L.
EDITORIAL TÉCNICA Y COMUNICACIÓN

Avda. Reina Victoria, 47
28003 Madrid (Spain)
Telf. +34-915 538 297
correo@ibanezyplaza.com
www.ibanezyplaza.com

Graphic design
Concha García García

English translation
David Shea

ISSN: 2173-2345

Submit originals:
romm@ibanezyplaza.com

Summary

Vol. 12 - Nº 2 - April-June 2020

Indexed in: Scielo, Web of Sciences, IBECS, Scopus, SIIC Data Bases, embase, Redalyc, Emerging Sources Citation Index, Open J-Gate, DOAJ, Free Medical Journal, Google Academic, Medes, Electronic Journals Library AZB, e-revistas, WorldCat, Latindex, EBSCOhost, MedicLatina, Dialnet, SafetyLit, Mosby's, Encare, Academic Keys, ERIH plus, British Library, ROAD.

Revista de Osteoporosis y Metabolismo Mineral has recently been acepted for coverage in the Emerging Sources Citation Index, wich is the new edition of the Web of Science that was launched in november 2015. This means that any articles published in the journal will be indexed in the Web of Science at the time of publication.

Editorial Committee

Rev Osteoporos Metab Miner. 2020;12(2):37-39

Methodology to improve the efficiency in the migration and detection of mesenchymal stem cells in murine models

DOI: http://dx.doi.org/10.4321/S1889-836X2020000200001

Naves Díaz M
Clinical Management Unit for Bone Metabolism. Asturias Central University Hospital (HUCA). Renal Research Network of the Carlos III Health Institute (REDinREN-ISCIII). Institute for Health Research of the Principality of Asturias (ISPA). Oviedo (Spain)

Osteoporosis is a generalised disease of the skeletal system characterised by an imbalance between the bone formation and resorption that leads to bone mass loss and to the deterioration of the microarchitecture of the bone tissue, compromising bone resistance and therefore resulting in a higher bone fragility and an increased susceptibility to fractures[1].

Two stem cells coexist in the bone cavity (bone marrow): the hematopoietic stem cell, which generates all the blood and immune system cells, and the mesenchymal stem cell, responsible for the formation of the skeleton. Osteoblasts or bone-forming cells originate from the differentiation of mesenchymal stem cells. These pluripotent cells can create a wide variety of cell types such as osteoblasts, adipocytes, or chondrocytes[2-4]. This characteristic makes them highly interesting candidates for regenerative medicine given their ability to migrate to injured areas to promote the de *novo* generation of bone[5].

The interest in the use of mesenchymal stem cells in the field of bone metabolism has grown in the early 2000s. Studies have focused primarily on the intravenous treatment of mesenchymal stem cells in children with osteogenesis imperfecta, an inherited enzyme deficiency in collagen synthesis by mesenchymal cells in the bones. This hypothesis is based on observing that bone marrow transplantation can provide stromal cells capable of synthesizing intact type I collagen, replacing the poor cellular function of the patient and improving the symptoms of the disease. The efficacy of the treatment was reported in a study carried out on six newborn children, showing better growth rates and initial intact bone synthesis[6]. In a second study, these same authors showed that autologous mesenchymal stem cells had normal collagen production in bone cavities, and that transplanted children had growth curves similar to those of transplanted children with allogeneic bone marrow[7]. This pioneering work has served as the basis for the successful application of intravenous mesenchymal stem cells in other clinical entities.

Once introduced into the body, mesenchymal stem cells initiate a process known as homing or nesting in which they are retained in the blood vessels of damaged tissue and are guided to the tissue from these blood vessels by biological mediators such as chemokines, cytokines and adhesion molecules.

To monitor transplanted human cells in animal models, cells previously tagged with a fluorophore are used to detect the signal *in vivo* via magnetic resonance imaging or positron emission tomography. An alternative to these imaging techniques is the detection by real-time quantitative PCR of the presence of transferred human DNA in the organ of interest using Alu elements, a name derived from the presence of a recognition site for the restriction enzyme Alu I.

To monitor transplanted human cells in animal models, cells previously tagged with a fluorophore are used to detect the signal in vivo via magnetic resonance imaging or positron emission tomography[8]. An alternative to these imaging techniques is the detection by real-time quantitative PCR of the presence of transferred human DNA in the organ of interest using Alu elements[9], a name derived from the presence of a recognition site for the restriction enzyme Alu I. These Alu elements are short sequences of about 300 base pairs, which are repeated throughout the genome, representing roughly 10% of the total. These characteristics and the fact that the appearance of these Alu sequences dates back approximately 65 million years, coinciding with the origin and expansion of

Correspondence: Manuel Naves Díaz (mnaves.huca@gmail.com)

primates, makes them ideal for detecting human cells[10]. However, the limits of detection of the current techniques for studying human genomic DNA do not allow it to be distinguished from other non-human DNA.

In this issue of the Journal of Osteoporosis and Mineral Metabolism, Del Real et al.[11] develop a methodology based on the work of Funakoshi et al., using a highly sensitive and specific quantitative real-time PCR method based on Alu sequences to discriminate human cells from rodent cells[12]. The aim of this work was to study, by means of PCR analysis of human Alu sequences, the performance to detect human DNA after the infusion of human bone marrow stem cells in immunodeficient mice. These human bone marrow stem cells were obtained from the femoral head of patients undergoing hip replacement surgery.

These authors were able to locate human DNA in the lungs of mice on the first day and 7 days after cell infusions, but this human DNA was inconsistently detected in the liver and the bones, presenting a discrete decrease in human DNA among the days 1 and 7 in the lung, but with clear differences in human DNA levels on day 1 compared to samples that did not contain human DNA.

The authors comment on the need to study the distribution of these cells after their infusion into the bloodstream, for which a very sensitive and specific method of detecting small populations of human cells among the cells of the recipient organism is needed. Based on the methodology developed by Funakoshi et al.[12], Del Real et al. were able to detect very low concentrations of human DNA among a high concentration of mouse DNA[11]. After intravenous infusion of human bone marrow stem cells into mice and between the first 24 hours and the seventh day, these authors were able to verify that human cells were only detectable in the lung, not consistently appearing in either the liver or the bones. As a consequence of this practical limitation, several strategies are being tested to increase the tropism of human bone marrow stem cells to bone tissue, using for this purpose the glycosylation of membrane proteins that allow greater attraction to bone[13].

Therefore, as previously mentioned, although the use of intravenously infused human mesenchymal cells for regenerative bone treatment is a very promising strategy, there are important methodological limitations as they can become trapped in the lungs and quickly lost. The search for procedures that selectively target these cells to the bone and the ability to improve their monitoring will, in the near future, open up a new therapeutic pathway for the treatment of osteoporosis.

Conflict of interest: The author declares that he has no conflicts of interest.

Bibliography

1. Díaz Curiel M. Osteoporosis: concepto. Fisiopatología. Clínica. Epidemiología. Rev Osteoporos Metab Miner. 2018;10 (1 Suplemento):2-4.
2. Pittenger MF, Mackay AM, Beck SC, Jaiswal RK, Douglas R, Mosca JD, et al. Multilineage potential of adult human mesenchymal stem cells. Science. 1999;284:143-7.
3. Caplan AI, Dennis JE. Mesenchymal stem cells as trophic mediators. J Cell Biochem. 2006;98:1076-84.
4. Caplan AI. Why are MSCs therapeutic? New data: new insight. J Pathol. 2009;217:318-24.
5. Han Y, Li X, Zhang Y, Han Y, Chang F, Ding J. Mesenchymal stem cells for regenerative medicine. Cells. 2019;8(8): 886.
6. Horwitz EM, Gordon PL, Koo WK, Marx JC, Neel MD, McNall RY, et al. Isolated allogeneic bone marrow-derived mesenchymal cells engraft and stimulate growth in children with osteogenesis imperfecta: implications for cell therapy of bone. Proc Natl Acad Sci U S A. 2002;99:8932-7.
7. Horwitz EM, Prockop DJ, Fitzpatrick LA, Koo WW, Gordon PL, Neel M, et al. Transplantability and therapeutic effects of bone marrow-derived mesenchymal cells in children with osteogenesis imperfecta. Nat Med. 1999;5:309-13.
8. Chikate TR, Tang L. Tracking and imaging of transplanted stem cells in animals. Methods Mol Biol. 2019; online ahead of print.
9. Schubert R, Sann J, Frueh JT, Ullrich E, Geiger H, Baer PC. Tracking of adipose derived mesenchymal stromal/stem cells in a model of cisplatin-induced acute kidney injury: Comparison of bioluminescence imaging versus qRTPCR. Int J Mol Sci. 2018;19(9): E2564.
10. Batzer MA, Deininger PL. Alu repeats and human genomic diversity. Nat Rev Genet. 2002;3(5):370-9.
11. Del Real A, López-Delgado L, Sañudo C, Pérez-Núñez MI, Laguna E, Menéndez G, et al. Método sensible para monitorizar la migración de las células madre mesenquimales de la médula ósea en modelos murinos. Rev Osteoporos Metab Miner. 2020;12(2):40-44.
12. Funakoshi K, Bagheri M, Zhou M, Suzuki R, Abe H, Akashi H. Highly sensitive and specific Alu-based quantification of human cells among rodent cells. Sci Rep. 2017;7(1): 13202.
13. Sackstein R, Merzaban JS, Cain DW, Dagia NM, Spencer JA, Lin CP, et al. Ex vivo glycan engineering of CD44 programs human multipotent mesenchymal stromal cell trafficking to bone. Nat Med. 2008;14(2):181-7.

Rev Osteoporos Metab Miner. 2020;12(2):40-44

A sensitive method for monitoring the migration of mesenchymal stem cells from bone marrow in murine models

DOI: http://dx.doi.org/10.4321/S1889-836X2020000200002

Del Real A[1], López-Delgado L[1], Sañudo C[1], Pérez-Núñez MI[2], Laguna E[2], Menéndez G[2], Garcés C[2], García-Montesinos B[3], García-Ibarbia C[1], Santurtún A[4], Riancho JA[1]

1 Internal Medicine Service. Marqués de Valdecilla University Hospital. University of Cantabria. Valdecilla Research Institute (IDIVAL). Santander (Spain)
2 Traumatology Service. Marqués de Valdecilla University Hospital. University of Cantabria. Valdecilla Research Institute (IDIVAL). Santander (Spain)
3 Maxillofacial Surgery Service. Marqués de Valdecilla University Hospital. Santander (Spain)
4 Legal Medicine Unit. University of Cantabria. Valdecilla Research Institute (IDIVAL). Santander (Spain)

Date of receipt: 23/01/2020 - Date of acceptance: 08/04/2020

This paper was awarded a scholarship to attend the 41st ASBMR Congress (Orlando, 2019)

Summary

Objetive: Mesenchymal stem cells (MSCs) are commonly used in regenerative therapy of human diseases. In murine models, in which human MSCs are transplanted, distinguishing the origin of the identified MSCs in the organs of mice is important. The objective of this study was to determine the performance of PCR-based analysis of human Alu sequences to detect human DNA after infusion of human bone marrow stem cells (hBMSCs) in immunodeficient mice.

Material and method: HBMSCs were obtained from the femoral head of patients undergoing hip replacement surgery. 10^6 hBMSCs were infused intravenously by injection into the retro-orbital sinus of NOD/SCID mice. The presence of human DNA in lung, liver and bone was then assessed.

Results: In *in vitro* DNA mixtures, human DNA was easily detected with a good logarithmic-linear relationship. Similarly, when human and mouse osteoblasts were mixed, 1-10 cells were easily detected among 10^5 mouse cells. Likewise, human DNA was detected in the lungs 1 and 7 days after cell infusions in NOD/SCID mice. However, human DNA was inconsistently detected in the liver and bones.

Conclusion: Detecting Alu sequences is an effective procedure to observe human DNA. The results confirm that most intravenously injected hBMSCs are trapped in the lungs. Thus, for the treatment of skeletal disorders, procedures are needed to increase the migration of these cells to the bone.

Key words: mesenchymal stem cells, osteoporosis, cell migration, regenerative therapy, Alu sequences.

Introduction

Osteoporosis is the most frequent bone disease, characterized by low bone mass and alteration of the microstructure. This is due to an imbalance between bone formation and bone resorption that causes loss of connections among the different bone trabeculae, a greater thinning and cortical bone porosity. Consequently, there is greater bone fragility and an increased risk of fractures (Fx)[1,2].

Osteoblasts, cells specialized in bone formation, originate from the differentiation of mesenchymal stem cells (MSCs)[3]. These cells are multipotent and can differentiate into a wide variety of mesoderm cell types, such as osteoblasts, adipocytes, or chondrocytes. MSCs are highly interesting candidates for regenerative medicine, because they migrate to skeletal lesions where they have the capacity to form new bone[4]. The many relevant published studies show the importance of MSCs in tissue engineering and regenerative medicine[5,6]. In addition, there are currently more than 250 clinical trials with MSCs, as reflected in the clinical trial database (clinicaltrials.gov).

Correspondence: José A. Riancho (jose.riancho@unican.es)

Imaging techniques such as magnetic resonance imaging and positron emission tomography, and cells previously labeled with a fluorophore are used to monitor transplanted human cells in animal models to detect the signal *in vivo*[7,8]. An alternative approach is to detect the presence of human DNA in *ex-vivo* animal models. So, once the treatment is complete, the presence of DNA of human origin is accessed in the target organ by real-time quantitative PCR (qPCR)[9-11]. Alu sequences or elements are short, repetitive, intercalating elements of the genome (SINE), approximately 300 base pairs in length. There are more than 1 million copies of Alu sequences in the human genome, occupying about 10% of the entire genome[12,13]. Given their small size, specific distribution among species and high number of copies, they are a very useful target for detecting human cells. However, most of the Alu-based experimental techniques to detect only human genomic DNA do not reach the limits of sensitivity and specificity necessary to distinguish them from DNA from other primates or rodents[13,14]. Funakoshi et al. have developed a highly sensitive and specific Alu-based quantitative real-time PCR method to discriminate human cells from rodent cells, to avoid possible cross-reactions[11].

The objective of this study was to determine the performance of PCR-based analysis of human Alu sequences to detect human DNA after infusion of human bone marrow stem cells (hBMSCs) in immunodeficient mice (NOD/SCID).

Material and methods

Isolation of hBMSCs

HBMSCs were obtained from the femoral head of patients undergoing hip replacement surgery. The study was approved by the Cantabria Clinical Research Ethics Committee and patients gave their written informed consent. Cylinders of trabecular bone were removed from the femoral head with a trocar and these were washed in PBS to obtain the bone marrow cells. Ficoll gradients were centrifuged to obtain the mononuclear layer, the one that was finally cultivated to attain an 80% state of confluence.

NOD/SCID mice and cell infusion

NOD/SCID immunodeficient mice, obtained from Charles River Laboratories International, Inc. (Wilmington, Massachusetts, USA), were injected with 10^6 hBMSCs intravenously infused into the retro-orbital sinus.

DNA isolation and real-time quantitative PCR

The mouse femur and human bone cylinders were homogenized with a polytron in lysis buffer and proteinase k, which was stored in an overnight incubation at 55°C with shaking. The soft tissues, lung and liver, were directly homogenized in lysis buffer and proteinase k. The DNA was then isolated with phenol: chloroform: isoamyl alcohol, and precipitated with 100% ethanol. The presence of human DNA in the DNA extracted from these organs (lung, liver and bone) was evaluated by real-time PCR, with a hybridization temperature of 56ºC for 40 cycles, using the primers and protocol proposed by Funakoshi[11] (Table 1).

Negative controls without DNA (NTC) and DNA extracted from mouse tissues without hBMSCs were included in all cases. Likewise, DNA extracted from artificial mixtures of human and mouse cells, as well as mixtures of purified human DNA and murine DNA, were analyzed. The threshold cycle (Ct) of each sample, that is, the amplification cycle from which the amplicons were detectable, was estimated. Logically, there is an inverse relationship between the amount of target DNA present in the sample and the Ct.

Table 1. Primers and the hydrolysis probe used to detect ALU sequences

Name	Sequence (5'→3')
Direct Primer (101 F)	5'-GGTGAAACCCCGTCTCTACT-3'
Reverse Primer (206 R)	5'-GGTTCAAGCGATTCTCCTGC-3'
Hydrolysis probe (144RH)	5'-CGCCCGGCTAATTTTTGTAT-3'

Written informed consent was obtained from patients who donated hBMSCs, in accordance with procedures approved by the Cantabria Clinical Research Ethics Committee. Regarding animal experiments, the protocol was approved by the Research Ethics Committee of the University of Cantabria and the Ministry of Health of Cantabria, as established by current regulations.

Results

Mixtures of human and mouse DNA

In the methods of detecting human DNA in a different organism, such as the mouse, high technical sensitivity and specificity are critical. For this, the first evaluation of the detection technique used in this article was carried out with DNA mixtures and with mixtures of different numbers of cells of human and mouse origin. A spectrophotometer (DeNovix DS-11, Wilmington, USA) was used to assess the amount of DNA in each sample. First, 100 ng/µL human DNA standard solutions were mixed with 100 ng/µL mouse DNA in a 1:1 ratio and up to 8 serial dilutions 1:10 were made in mouse DNA. Thus, progressive dilutions of human DNA obtained in the presence of mouse DNA practically constant. The expression levels on the Ct scale were 11.5; 14.6; 17.2; 21.0; 23.8; 26.8; 30.0; 32.5 and 33.6; for 100 ng/µL, 10 ng/µL, 1 ng/µL, 0.1 ng/µL, 0.01 ng/µL, 1 pg/µL, 0.1 pg/µL, 0.01 pg/µL and 0.001 pg/µL of human DNA, respectively (r^2=0.992; p<0.0001) (Figure 1). In several independent experiments, the threshold cycle (Ct) for NTC was 34.6±1.8, so 31 (2 standard deviations below the NTC mean) were considered as the maximum Ct to consider positive. the presence of human DNA in a sample. No signal was detected when up to 100 ng of mouse-only DNA was analyzed (Ct was 34.7±1.6).

Subsequently, human and mouse osteoblasts were mixed in different proportions prior to DNA extraction to simulate the technique in a real way. The 10 human cells were easily detected in a mixture of 10^5 mouse cells (Ct 25.6) and even a single cell was close to the detection limit (Ct 30.8) (Figure 2).

Analysis of human DNA in mouse tissues

Tissues from non-fractured NOD/SCID mice treated with intravenous hBMSCs were then analyzed. These levels were also compared with those detected in diluted human bone DNA samples, as positive controls. Human DNA could be located in the lungs on the first day and 7 days after cell infusions (Ct 22.6±0.7 and 30.6±3.7, respectively). However, human DNA was inconsistently de-

Figure 1. A) Detection of different concentrations of human DNA in a high concentration of mouse DNA. B) The same results using a logarithmic scale on the axis of abscissa indicate the expected log-linear relationship. The figure indicates the r^2 value of the Pearson regression and the significant p value for the linear regression. The broken line in A) and B) shows the threshold value of detection of DNA of human origin when mixing different concentrations

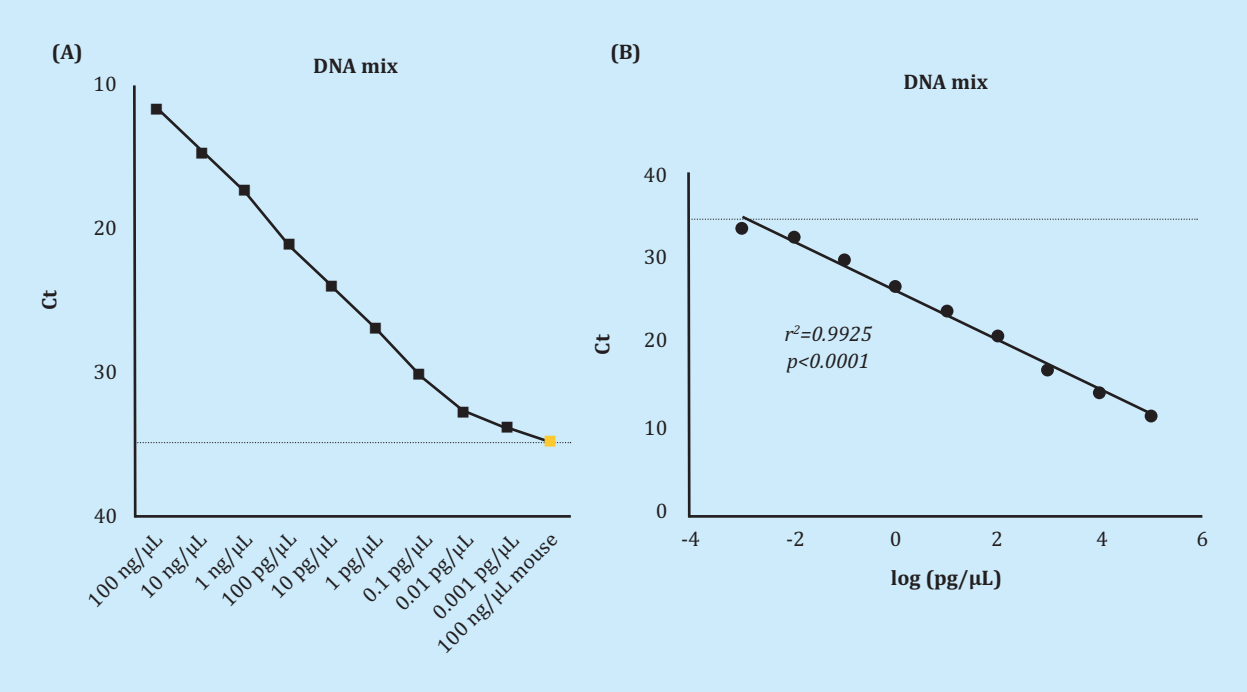

Figure 2. Amplification curve of qPCR with DNA obtained from different mixtures. The mixtures start from different numbers of cells of human origin mixed with 10^5 mouse cells. The broken line shows the threshold value for detection of DNA of human origin

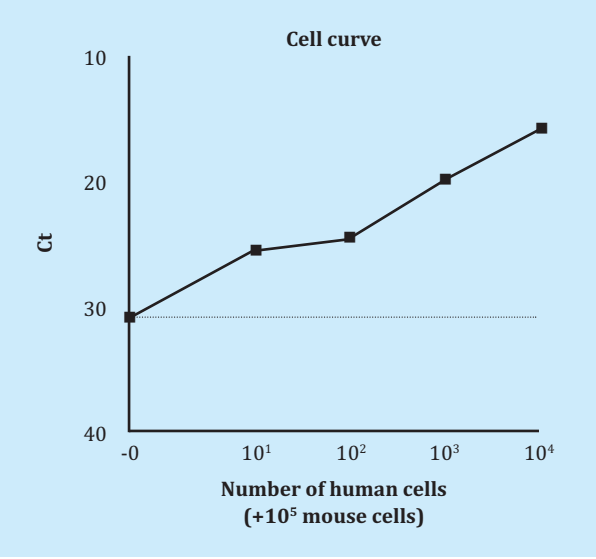

tected in the liver and bones (Figure 3). There is a decrease in human DNA between days 1 and 7 in the lung samples, but these differences are not significant. However, when comparing day 1 human DNA levels with samples without DNA they are significant (Figure 4).

Discussion

Reparing bone fractures is a complex process, where there are a series of molecular mechanisms regulated by various factors that lead to new bone formation. This repair can sometimes be altered by aging and by different bone disorders, such as osteoporosis or avascular necrosis, among others[5]. Regenerative therapy attempts to solve these imbalances by avoiding allogeneic transplant rejection and adverse immune reactions. For this, new osteoinductive biomaterials, osteogenic regulation factors and MSCs[15] have been used. These are of great interest and numerous studies involving MSCs have been published. MSCs are characterized by having a high capacity for renewal and also being able to form new cell types of mesodermal origin, such as osteoblasts or adipocytes. Furthermore, they have immunomodulatory effects and secrete factors that induce cell differentiation[5,16].

The physiological function and repair capacity of human MSCs are commonly studied in xenografts carried out in rodents. After intravenous xenotransplantation, cells can circulate widely throughout the body and their tropism by different organs needs to be studied. Consequently, it is necessary to study these cells' distribution after blood infusion. To do so, a highly sensitive, specific method of detecting small populations of human cells among the cells of the recipient organism is needed. Funakoshi et al. have developed a qPCR system, theoretically very sensitive and specific, that allows us to detect these small populations of human MSCs that have survived after their infusion in mice. The mechanism, based on Alu sequences that differ from each other in terms of species evolution and can specifically detect those of uniquely human origin[11]. Due to the extremely high number of copies of the Alu sequence in the human genome, a single primer could amplify the inter-Alu genomic sequence, which can result in the formation of amplified products with unpredictable and complex pat-

terns. To minimize the effects of such non-specific signals, the method uses hydrolysis probes, which hybridize to the sequence to be amplified between both primers. Still, in this reaction there are nonspecific hybridizations to the mouse genome that cause an unavoidable background fluorescence signal, which is considered technical noise. Our objective was to confirm the usefulness of this methodology in our model.

In fact, with this procedure we were able to detect very low concentrations of human DNA among a high concentration of mouse DNA, specifically up to 0.01 pg/µL of human DNA between 100 ng/µL of mouse. In cell mixtures, the detection threshold was 1-10 human cells in 10^5 mouse cells.

HBMSCs were injected intravenously into mice. This procedure verified that, after the first 24 hours and the seventh day, they were only detectable in the lung (they were not consistently detected in liver or bone). Various strategies are being tested to increase the tropism of hBMSCs to bone tissue. One of them is based on modifying membrane proteins, with specific glycosylation particles that allow extravasation and a greater tropism for bone[17].

In conclusion, the results confirm that the majority of hBMSCs injected intravenously into NOD/SCID mice are trapped in the lungs and are rapidly lost. Therefore, procedures are needed to increase the tropism of these cells to bone if hBMSCs are to be used in systemic regenerative skeletal procedures.

Financing: This project was funded by the Carlos III Health Institute (PI16/915).

Figure 3. Detection of human Alu sequences in different mouse tissues 1 and 7 days after infusion of BMSCs intravenously. In orange are the control samples to which no cells were injected. The broken line shows the threshold value for detection of DNA of human origin. (●) Liver; (▪) Lung; (▲) Bone. Day 1 geometric figures show the mean of 3 mice; those of day 7 of 4 mice; and those without cells from 2 mice. The downward triangles (▼), green in color, are samples of bone of human origin

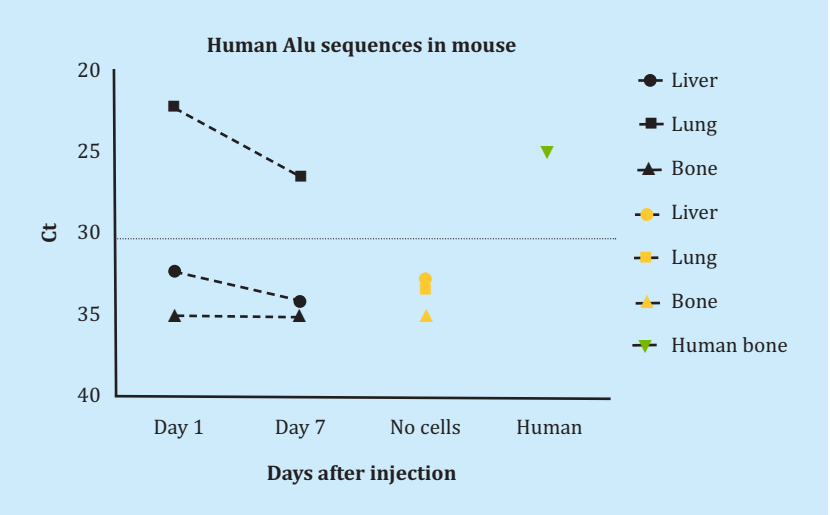

Figure 4. Detection of human Alu sequences in mouse lung 1 and 7 days after infusion of BMSCs intravenously. In orange are the control samples to which no cells were injected. The broken line shows the threshold value for detection of DNA of human origin

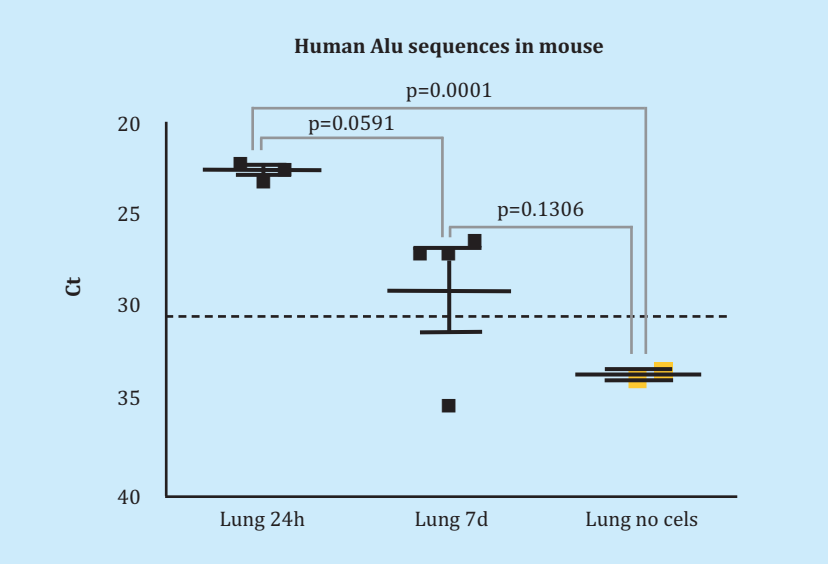

Conflict of interests: Authors declare no conflict of interests.

Bibliography

1. Eastell R, O'Neill TW, Hofbauer LC, Langdahl B, Reid IR, Gold DT, et al. Postmenopausal osteoporosis. Nat Rev Dis Prim. 2016;2(1):16069.
2. Díaz Curiel M. Osteoporosis: concepto. Fisiopatología. Clínica. Epidemiología. Rev Osteoporos Metab Miner. 2018;10 (1 Suplemento):2-4.
3. Katsimbri P. The biology of normal bone remodelling. Eur J Cancer Care. (Engl). 2017;26(6).
4. Han Y, Li X, Zhang Y, Han Y, Chang F, Ding J. Mesenchymal stem cells for regenerative medicine. Cells. 2019;8(8):886.
5. Iaquinta MR, Mazzoni E, Bononi I, Rotondo JC, Mazziotta C, Montesi M, et al. Adult stem cells for bone regeneration and repair. Front Cell Dev Biol. 2019; 7:268.
6. Brown C, McKee C, Bakshi S, Walker K, Hakman E, Halassy S, et al. Mesenchymal stem cells: Cell therapy and regeneration potential. J Tissue Eng Regen Med. 2019 Sep;13(9):1738-55.
7. Freeman BT, Kouris NA, Ogle BM. Tracking fusion of human mesenchymal stem cells after transplantation to the heart. Stem Cells Transl Med. 2015; 4(6):685-94.
8. Chikate TR, Tang L. Tracking and imaging of transplanted stem cells in animals. Methods Mol Biol. 2019; online ahead of print.
9. Creane M, Howard L, O'Brien T, Coleman CM. Biodistribution and retention of locally administered human mesenchymal stromal cells: Quantitative polymerase chain reaction–based detection of human DNA in murine organs. Cytotherapy. 2017;19 (3):384-94.
10. Schubert R, Sann J, Frueh JT, Ullrich E, Geiger H, Baer PC. Tracking of adipose-derived mesenchymal stromal/stem cells in a model of cisplatin-induced acute kidney injury: Comparison of bioluminescence imaging versus qRT-PCR. Int J Mol Sci. 2018;19(9):E2564.
11. Funakoshi K, Bagheri M, Zhou M, Suzuki R, Abe H, Akashi H. Highly sensitive and specific Alu-based quantification of human cells among rodent cells. Sci Rep. 2017;7(1):13202.
12. Salem A-H, Kilroy GE, Watkins WS, Jorde LB, Batzer MA. Recently integrated Alu elements and human genomic diversity. Mol Biol Evol. 2003;20(8):1349-61.
13. Batzer MA, Deininger PL. Alu repeats and human genomic diversity. Nat Rev Genet. 2002;3(5):370-9.
14. Jurka J. Evolutionary impact of human Alu repetitive elements. Curr Opin Genet Dev. 2004;14(6):603-8.
15. Iaquinta MR, Mazzoni E, Manfrini M, D'Agostino A, Trevisiol L, Nocini R, et al. Innovative biomaterials for bone regrowth. Int J Mol Sci. 2019;20(3):618.
16. Abdel Meguid E, Ke Y, Ji J, El-Hashash AHK. Stem cells applications in bone and tooth repair and regeneration: New insights, tools, and hopes. J Cell Physiol. 2018;233(3):1825-35.
17. Sackstein R, Merzaban JS, Cain DW, Dagia NM, Spencer JA, Lin CP, et al. Ex vivo glycan engineering of CD44 programs human multipotent mesenchymal stromal cell trafficking to bone. Nat Med. 2008;14(2):181-7.

Rev Osteoporos Metab Miner. 2020;12(2):45-52

Can 3D measurements obtained by lumbar DXA predict fractures in the dorsal vertebrae?

DOI: http://dx.doi.org/10.4321/S1889-836X2020000200003

López Picazo M[1,2], Humbert L[1], Di Gregorio S[3], González Ballester MA[2,4], Del Río Barquero LM[3]
1 Musculoskeletal Unit. Galgo Medical. Barcelona (Spain)
2 BCN Medtech (Barcelona Center for New Medical Technologies). Pompeu Fabra University. Barcelona (Spain)
3 CETIR Grupo Médico. Barcelona (Spain)
4 ICREA (Catalan Institution for Research and Advanced Studies). Barcelona (Spain)

Date of receipt: 28/06/2019 - Date of acceptance: 27/02/2020

Work awarded with a scholarship to attend the 40th ASBMR Congress (Montreal, 2018)

Summary

Objective: To assess the relation between three-dimensional (3D) measurements obtained by lumbar dual energy X-ray absorptiometry (DXA) and osteoporotic fractures in dorsal vertebrae.

Material and methods: We analysed retrospectively 32 postmenopausal women, allocated to two groups: 16 women in the experimental group, who presented incident fractures of the dorsal vertebrae, and 16 women in the control group, who did not show any type of fracture. Measurements of the (aBMD) of vertebrae L1 through L4 were taken at the initial visit (i.e., prior to the fracture event) by lumbar dual-energy x-ray absorptiometries (DXA). 3D measurements obtained by DXA were evaluated using 3D modelling software (3D-SHAPER). Volumetric bone mineral density (vBMD) was calculated in the trabecular, cortical and integral bone. Cortical thickness and cortical surface BMD (sBMD) were also measured. Differences in measurements derived from the DXA between the experimental and control groups were assessed using an unpaired Student t-test. The odds ratio (OR) and the area under the receiver operating characteristic curve (AUC) were also determined.

Results: In the present age-adjusted case-control study, no significant differences were found between the experimental and control groups in terms of weight (ρ=0.44), height (ρ=0.25) and aBMD (ρ=0.11). However, significant differences (ρ<0.05) were found in the integral and trabecular vBMD and in the cortical sBMD. Trabecular vBMD in the vertebral body was the measure that best discriminated between both groups, with an AUC of 0.733, compared to 0.682 of the aBMD.

Conclusion: This study shows the ability of 3D models resultant from lumbar DXAs to discern between subjects with incident fractures in the dorsal vertebrae and control subjects. It is necessary to analyse larger cohorts to establish if these measurements could improve the prediction of fracture risk in clinical practice.

Key words: 3D modelling, fracture risk, osteoporosis, trabecular, cortical, vertebral fracture, volumetric bone mineral density, superficial bone mineral density.

Introduction

Every year 8.9 million osteoporosis-related fractures occur worldwide, representing one fracture every 3 seconds[1], with vertebral being the most common osteoporotic fractures[2].

Dual-energy X-ray absorptiometry (DXA) is the standard test for diagnosing osteoporosis and evaluating fracture risk[3,4], as it is a low-radiation, inexpensive technique. The DXA provides two-dimensional (2D) images that measure the bone mineral density of the area (aBMD) projected along the anteroposterior (AP) direction. Various studies show that a low aBMD value, measured in AP DXA explorations, is among the highest fracture risks[3-5]. The decrease of the aBMD standard deviation leads to an increase from 1.5 up to 3.0 times the risk of fracture, depending on its location and its measurement's location[5]. Nevertheless, a low BMD value is not enough to explain every fracture. Recent studies suggest that the risk of fracture is high when the BMD value is low, but this does not mean that fracture risk is negligible when the BMD value is normal[3-8].

Correspondence: Mirella López Picazo (mirella.lopez.picazo@gmail.com)

Most osteoporosis-related vertebral fractures are located in the vertebral body[9]. In AP DXA images of the spinal column, the vertebral body overlaps the posterior vertebral elements, so the BMD in the vertebral body cannot be estimated separately. On the other hand, the risk of fracture depends on the architecture of the trabecular bone and the thickness of the cortical bone[10]. However, the trabecular and cortical bone compartments are difficult to assess separately on AP DXA scans.

As an alternative to the DXA, quantitative computed tomography (QCT) provides a three-dimensional (3D) analysis of the bone structures. In QCT imaging, the volumetric BMD (vBMD) can be measured in the vertebral body alone, separate from the posterior vertebral elements, and even trabecular and cortical structures can be evaluated in isolation[3,11,12]. Previous studies have appraised the association between vBMD derived from QCT and vertebral fractures[8,13-17]. Finite element models based on QCT have also been analysed to know the mechanical properties of the vertebrae and to predict the risk of vertebral fracture[17-20]. However, QCT scans compared to DXA scans involve exposure to a higher dose of radiation, as well as a higher cost. As a consequence, QCT is rarely used in clinical practice for fracture risk assessment.

In order to overcome the limitations of the DXA and QCT scans, various researches suggest the use of 3D modelling methods to determine the shape and distribution of bone density considering a limited number of DXA scans[21-25]. These studies use a three-dimensional statistical model of the bone shape and density which is recorded in DXA examinations to obtain a personalized 3D model of such bone (QCT type). The precision of these methods[21-25] has been evaluated by comparing 3D models and measurements obtained via DXA and QCT. However, as far as we know, no study has been conducted on the association of measurements provided by DXA-based 3D modelling techniques and vertebral fractures.

On another note, AP DXA usually includes only the lumbar region (L1 to L4), since the rib cage overlaps in the projection, avoiding the use of DXA to determine the aBMD in the thoracic spine. Despite this, various studies indicate that the greatest number of vertebral fractures related to osteoporosis occur at the thoracoabdominal junction (T12-L1)[15,26]. Although the reason for this higher prevalence is unknown, it has been suggested that thoracic kyphosis and rib cage stiffness predispose this area to fracture as the vertebral load is higher at this location. Even though measurements made at the same fracture location show a greater power of discrimination, Budoff et al.[27] found a high correlation between trabecular vBMD in the lumbar vertebrae and trabecular vBMD in the dorsal vertebrae.

The objective of this study was to assess the ability of 3D measurements derived from the DXA to distinguish subjects with incident fractures of the dorsal vertebrae from control subjects. To do this, a retrospective case-control study was carried out, which included postmenopausal Caucasian females who experienced a fracture event in the dorsal vertebrae (cases) and control females of the same age without any type of fracture. For each subject, 3D measurements derived from lumbar DXA were obtained at the initial baseline visit (which took place at least one year prior to the vertebral fracture event for subjects in the experimental group) using lumbar DXA AP scans and a DXA-based 3D modelling technique[25].

Materials and methods

Study population

We analyzed in retrospect a database compiled at CETIR Grup Mèdic (Barcelona, Spain). The database is made up of postmenopausal Caucasian women over the age of 40 who have already had an initial baseline and follow-up visit, both conducted between the years 2000 and 2010. Subjects in the database were stratified into two groups: patients with incident fractures in the dorsal vertebrae related to osteoporosis (experimental group) and subjects without any type of fracture (control group). The inclusion criteria in the experimental group were: absence of prevalent osteoporotic fractures, incident osteoporotic fracture of the dorsal vertebrae during the follow-up period (between one and ten years from the initial baseline visit), and absence of non-vertebral osteoporotic fractures during the follow-up period. The inclusion criteria in the control group were: absence of any type of osteoporotic fracture at the time of the initial baseline visit and for at least seven years following it. The individuals in both groups were excluded if they had undergone spinal surgery or had any bone disease other than osteoporosis, such as severe osteoarthritis, severe scoliosis, spondylitis, spinal infection, or abnormal bone growth. Each subject in the experimental group was age-matched (± 5 years) with a subject in the control group (1:1). Clinical parameters such as age, weight, height, and body mass index (BMI) were collected from each subject at the initial baseline visit. The database used in this study is part of a previous study in which the relation between 3D measurements derived from lumbar DXA and different types of vertebral fractures was evaluated[28].

Vertebral fractures were confirmed by a radiologist, who used the evaluation of vertebral fractures according to the Genant semi-quantitative classification criteria[9]. The absence of fracture was determined by reviewing the clinical history of the subjects, analyzing the AP DXA examinations at the baseline and follow-up visits, and ruling out the subjects whose height decreased by 2 cm or more between the reference visit and the follow-up visit. The presence (experimental group) or absence (control group) of fractures in the dorsal vertebrae could not be confirmed by morphometry for all the subjects, so the study is limited to clinical fractures.

This study was conducted as stipulated by the latest version of the Declaration of Helsinki. The Scientific Committee of the CETIR Grup Mèdic gave its ethical approval for the use of retrospective clinical data and the measurement results within the scope of this study. Anonymity of each subject was ensured and maintained by using numerical codes for all records.

Medical images and 2D measurements derived from DXA

All the subjects included in the study went through a lumbar AP DXA examination at the baseline visit. DXA scans were carried out with a Prodigy densitometer (GE Healthcare, Madison, Wisconsin, USA) and analysed with the enCORE software (v14.10, GE Healthcare, Madison, Wisconsin, USA). DXA scans and analyses were performed by a radiologist at CETIR Grup Mèdic in accordance with the manufacturer's recommendations. 2D measurements derived from DXA, such as aBMD (in g/cm^2), bone mineral content (BMC, in g), and area (in cm^2), were measured for L1 to L4 vertebrae in the AP DXA examinations. The T-score was evaluated using the GE-Lunar reference curves for Spain.

3D measurements derived from the DXA

3D measurements derived from the DXA in the L1-L4 segment were obtained with 3D-SHAPER software (Galgo Medical, Barcelona, Spain) and AP DXA scans taken at the initial baseline visit (before fracture). 3D-SHAPER calculates a custom 3D model of the lumbar spine shape and density from a single AP DXA image, as described in López Picazo et al.[25] and is briefly summarized next. First, the custom 3D estimate is obtained by registering and fitting a statistical model of shape and density in the AP DXA image. The statistical model is previously generated using a training database of QCT scans of Caucasian men and women. The cortical bone of the vertebral body is then segmented using an algorithm based on intensity models[25,29]. This algorithm calculates the density profile along the normal vector at each node of the 3D surface mesh and adjusts it to a function defined by the thickness and cortical density, the location of the cortical cortex, the density of the surrounding tissues and the blur of the image. Finally, 3D measurements derived from the DXA are taken in different vertebral regions and bone compartments. The vBMD (in mg/cm^3), the BMC (in g) and the volume (in cm^3) were measured in the integral bone of the total vertebra and the vertebral body. These same measurements were also obtained for the trabecular and cortical compartments in the vertebral body. The average cortical thickness (Cort. Th., in mm) and the cortical surface bone mineral density (cortical sBMD, in mg/cm^2) were measured in the vertebral body. Cortical sBMD is the amount of cortical bone per unit area integrated along the normal vector at each node of the vertebral body surface mesh. It was calculated as the multiplication of the cortical vBMD (in mg/cm^3) and the Cort. Th. (in cm).

Statistical analysis

Descriptive statistics, including mean and standard deviation, were used to analyze both the experimental and control groups at the initial baseline visit. The differences between the groups were assessed using the unpaired Student t-test, after verifying the normality of the data. A value of $p<0.05$ was considered statistically significant. Invariant logistic regressions were used to investigate possible correspondence between independent variables (weight, height, BMI, 2D and 3D measurements obtained by DXA) and the state of the fracture. The ability of DXA-derived measurements to discriminate between subjects with fractures and control subjects was assessed using the area under the receiver operating characteristic curve (AUC). The odd ratio (OR) was calculated with 95% confidence intervals (CI) to estimate the odds of a vertebral fracture occurring at any change of one standard deviation in measurements obtained by the DXA. The mean of the 3D shape and the density to visualize the differences in the distribution of vBMD were calculated for each group. Cuts in the median plane of the vertebral body were used to display the anatomical distribution of the differences in vBMD. The distribution of cortical sBMD was also calculated for each group. The differences in cortical sBMD distribution were shown in one instance of the average shape. Statistical analyses were carried out using Matlab Academic (version R2015b, MathWorks, Inc., Natick, Massachusetts, USA).

Results

Characteristics of the subjects

32 postmenopausal Caucasian women were included in this study: 16 patients with at least one incident osteoporotic fracture of the dorsal vertebrae (experimental group) and 16 subjects of the same age without any type of fracture (control group). The fractured group consisted of 11 subjects with a single fractured dorsal vertebra and 5 subjects with multiple vertebral fractures. A total of 25 incident vertebral fractures were found in the patients in the fracture group: two T4, two T7, one T8, one T9, three T10, one T11, nine T12, five L1 and one L2. It is unknown whether the vertebral fractures presented wedge, biconcave or crush deformities.

Patients in the experimental group had a vertebral fracture event at an average (± standard deviation) of 3.2±2.4 years from the initial baseline visit. The absence of osteoporotic fracture events was ensured for the controls during an average period of 8.4±1.0 years. No significant differences ($\rho \geq 0.05$) were observed between the experimental and control groups in terms of age, weight, height and BMI (Table 1).

2D measurements derived from DXA

In line with WHO classification criteria, 94% of the patients in both groups presented a low aBMD (T-score for L-L4 <-1). The experimental group included 12 women with osteoporosis, 3 with low bone mass and 1 with normal bone mass; while the control group included 5 women with osteoporosis, 10 with low bone mass and 1 with normal bone mass.

The mean aBMD in the L1-L4 segment of the subjects in the experimental group was 8.1% lower compared to those in the control group, although not significant ($p=0.11$; table 2). There were also no significant differences in BMC and AREA ($p>0.05$). The aBMD differentiated between the experimental group and the control group with an AUC=0.662. Each decrease in one standard deviation in the aBMD was associated with an almost two-fold increase in the probability of presenting an osteoporotic fracture in the dorsal vertebrae (OR=1.862; 95% CI: 0.862-4.022).

Table 1. Characteristics of the subjects at the initial baseline visit

	Controls	Fractured	p*
Number	16	16	
Age (years)	63.9 ± 7.7 [50.0 - 74.0]	64.9 ± 8.4 [48.8 - 75.7]	0.738
Weight (kg)	61.7 ± 10.1 [46.0 - 85.0]	64.2 ± 8.2 [54.0 - 83.0]	0.444
Height (cm)	154.0 ± 4.7 [143.0 - 161.0]	156.0 ± 5.1 [148.0 - 169.5]	0.251
BMI (kg/m^2)	26.0 ± 3.6 [21.0 - 32.8]	26.4 ± 2.9 [22.0 - 30.8]	0.733

Results expressed as mean ± standard deviation [minimum - maximum]; *: p values of the unpaired Student t-test; BMI: body mass index.

3D measurements derived from the DXA

The integral vBMD in the total vertebra in the experimental group was 10.2% lower than in the control group (p<0.05; table 2). In the vertebral body, the differences in vBMD were more pronounced in the trabecular bone (-16.2%, p<0.01) than in the integral bone (-12.8%, p<0.01). Cortical vBMD in the vertebral body was 2.3% lower in the experimental group, as well as non-significant (p=0.477). The cortical vBMD in the vertebral body in the experimental group was 10.0% lower than in the control group (p=0.018). The anatomical distribution of the mean differences between the trabecular vBMD in the vertebral body of the subjects included in the fractured and control groups is shown in figure 1. In it, we can see how the differences in the trabecular vBMD are more pronounced near the end plates of the vertebral body.

The trabecular vBMD in the vertebral body was related to higher values of AUC (0.801) and OR (5.060; 95% CI: 1.406-18.208), compared to other measurements derived from DXA (Table 2). Slightly lower values were found for the integral vBMD in the vertebral body (AUC=0.793 and OR=4.557; 95% CI: 1.411-14.718). The AUC map associated with the trabecular vBMD values calculated at each voxel of the volumetric images of the subjects included in the experimental and control groups is shown in figure 2. Only the AUC of the 90th percentile (AUC>0.720) are represented. A maximum AUC value of 0.815 was reached. Trabecular vBMD measurements show a higher AUC value near the end plates.

Cortical sBMD in the vertebral body was connected to higher values of AUC (0.734) and OR (2.649; 95% CI: 1.111-6.313), compared to other measurements made on cortical bone (Table 2). The anatomical distribution of the mean differences in cortical sBMD between the subjects included in the experimental and control

Table 2. Measurements derived from the DXA of the initial baseline visit in both groups, differences between groups, AUC and OR

L1-L4	Controls	Fractured	Differences	p*	AUC	OR [IC 95%]
2D measurements derive from DXA						
aBMD	0.931 ± 0.126	0.856 ± 0.133	-0.076 (-8.1%)	0.110	0.662	1.862 [0.862 - 4.022][a]
BMC	46.6 ± 7.8	44.4 ± 9.6	-2.7 (-5.8%)	0.392	0.613	1.382 [0.672 - 2.841][a]
Area	50.0 ± 3.9	51.1 ± 6.2	1.2 (2.4%)	0.523	0.488	0.785 [0.382 - 1.614][b]
3D measurements derived from the DXA						
Integral bone, total vertebra						
Int. vBMD	256.2 ± 36.6	230.0 ± 34.0	-26.2 (-10.2%)	**0.044**	0.691	2.296 [0.974 - 5.413][a]
Int. BMC	40.5 ± 6.9	38.1 ± 8.4	-2.4 (-6.0%)	0.379	0.602	1.394 [0.677 - 2.868][a]
Int. volume	157.9 ± 14.1	165.2 ± 23.7	7.3 (4.6%)	0.300	0.574	0.670 [0.317 - 1.417][b]
Integral bone, vertebral body						
Int. vBMD	207.6 ± 24.1	181.0 ± 20.5	-26.6 (-12.8%)	**0.002**	0.793	4.557 [1.411 - 14.718][a]
Int. BMC	21.3 ± 3.1	19.2 ± 3.9	-2.1 (-9.7%)	0.109	0.652	1.865 [0.863 - 4.029][a]
Int. volume	102.6 ± 9.3	105.8 ± 15.5	3.2 (3.1%)	0.484	0.531	0.766 [0.371 - 1.583][b]
Trabecular bone, vertebral body						
Trab. DMOv	134.5 ± 21.2	112.7 ± 16.3	-21.8 (-16.2%)	**0.003**	0.801	5.060 [1.406 - 18.208][a]
Trab. BMC	12.0 ± 2.0	10.5 ± 2.0	-1.5 (-12.7%)	**0.038**	0.688	2.338 [0.996 - 5.486][a]
Trab. volume	89.4 ± 8.7	93.3 ± 13.8	3.8 (4.3%)	0.357	0.563	0.702 [0.334 - 1.473][b]
Cortical bone, vertebral body						
Cort. vBMD	704.3 ± 47.9	687.9 ± 77.2	-16.3 (-2.3%)	0.477	0.543	1.307 [0.639 - 2.673][a]
Cort. BMC	9.3 ± 1.4	8.7 ± 2.2	-0.6 (6%)	0.401	0.570	1.373 [0.668 - 2.823][a]
Cort. volume	13.2 ± 1.3	12.5 ± 1.9	-0.6 (-4.7%)	0.294	0.621	1.492 [0.716 - 3.110][a]
Cort. Th.	0.66 ± 0.06	0.62 ± 0.05	-0.05 (-7.1%)	**0.017**	0.734	2.659 [1.115 - 6.342][a]
Cort. BMDs	52.2 ± 6.5	47.0 ± 5.1	-5.2 (-10.0%)	**0.018**	0.734	2.649 [1.111 - 6.313][a]
Cortical bone, regions of the vertebral body						
Cort. BMDs (Higher)	58.7 ± 8.0	52.5 ± 5.8	-6.3 (-10.7%)	**0.017**	0.730	2.722 [1.115 - 6.644]
Cort. BMDs (Lower)	56.9 ± 6.8	51.5 ± 5.7	-5.3 (-9.4%)	**0.023**	0.754	2.793 [1.060 - 7.358]
Cort. BMDs (Previous)	41.1 ± 7.4	35.9 ± 5.9	-5.3 (-12.8%)	**0.035**	0.699	2.363 [1.020 - 5.477]
Cort. BMDs (Later)	54.1 ± 8.8	50.1 ± 8.8	-4.0 (-7.4%)	0.209	0.637	1.629 [0.762 - 3.480]

Measurements of the experimental and control groups are expressed as mean ± standard deviation. Differences between groups are expressed as mean (percentage). *: p values of the unpaired Student t-test; p values <0.05 are shown in bold; [a]: probability ratio corresponding to a standard deviation of decrease in the measure; [b]: probability ratio corresponding to a standard deviation of increase in the measurement; AUC: area below the receiver operating characteristic curve; OR: odds ratio; CI: confidence interval; Int.: integral; Trab.: trabecular; Cort.: cortical; aBMD: areal bone mineral density (g/cm^2); BMC: bone mineral content (g); area (cm^2); vBMD: volumetric bone mineral density (mg/cm^3); volume (cm^3); Cort. Th .: cortical thickness (mm); BMDs: surface bone mineral density (mg/cm^2); Int.: integral bone; Trab.: trabecular bone; Cort.: cortical bone; Total: total vertebra; Body: vertebral body.

groups, is shown in figure 3 (top). More pronounced differences (magenta-coloured) were found in the end plates of the L1, L2 and L4 vertebrae. The cortical sBMD in the lower end plate was the measure of sBMD with the highest AUC (0.754) and OR (2.793; 95% CI: 1.060-7.358) values. Figure 3 (bottom) shows the AUC value calculated using cortical sBMD at each vertex of the vertebral body surface. AUC values of the 90th percentile (i.e. in the range of 0.777-0.836) are circled in red and were found mainly on the end plates.

Discussion

In the present study, the ability of 3D measurements derived from lumbar DXA, to discriminate between postmenopausal women with and without osteoporotic fractures in the dorsal vertebrae, was evaluated. 3D measurements derived from the DXA were performed at the initial baseline visit (at least one year before the vertebral fracture event), using standard DXA scans and a 3D modelling technique[25].

Age, gender, and BMI are independent risk factors for osteoporosis-related fractures[3,4]. In this study, a database of postmenopausal females paired by age was used to eliminate the possible effect of age and gender on the results. Although inclusion criteria related to height or weight were not used to recruit subjects, no significant differences were found between the groups in terms of height, weight, and BMI at the initial baseline visit.

No significant differences were observed in the aBMD (-8.1%, p=0.110), but in the integral vBMD (-10.2%, p=0.044). On the other hand, higher ORs were found for the vBMD measurements obtained via DXA in the verte-

Figure 1. Anatomic distribution of the mean differences in trabecular vBMD, between the subjects included in the experimental group and those in the control group. The differences are shown in the mid-coronal plane (centre) and the median lateral plane (right) of the vertebral body. The image on the left shows the plans that were used. The red-yellow areas indicate the regions where the difference in trabecular vBMD between the subjects with vertebral fracture and the control subjects is on average lower (in blue-green areas this difference is higher). Non-significant changes (unpaired Student t-test) were marked in black. The pink outline indicates the periosteal surface of the vertebral body

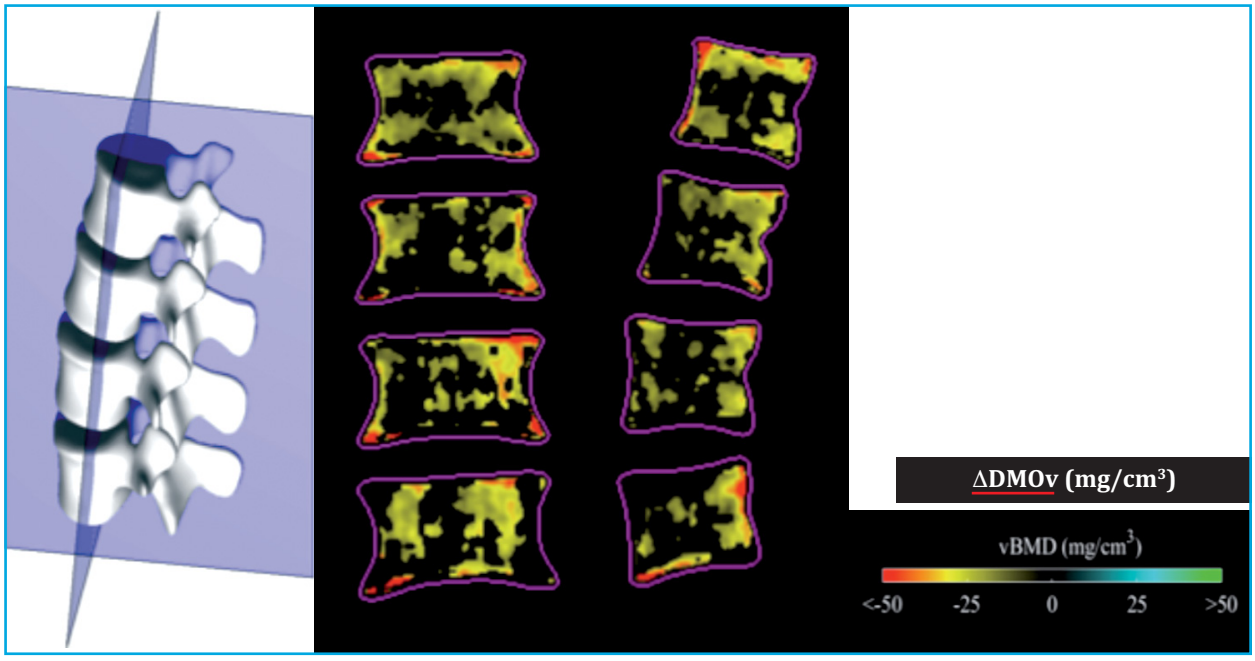

Figure 2. Map of the AUC calculated by using the trabecular vBMD in each voxel of the volumetric images of the subjects included in the experimental group and the control group. Only AUCs greater than the 90th percentile are represented (AUC >0.778). The maximum AUC registered is 0.930

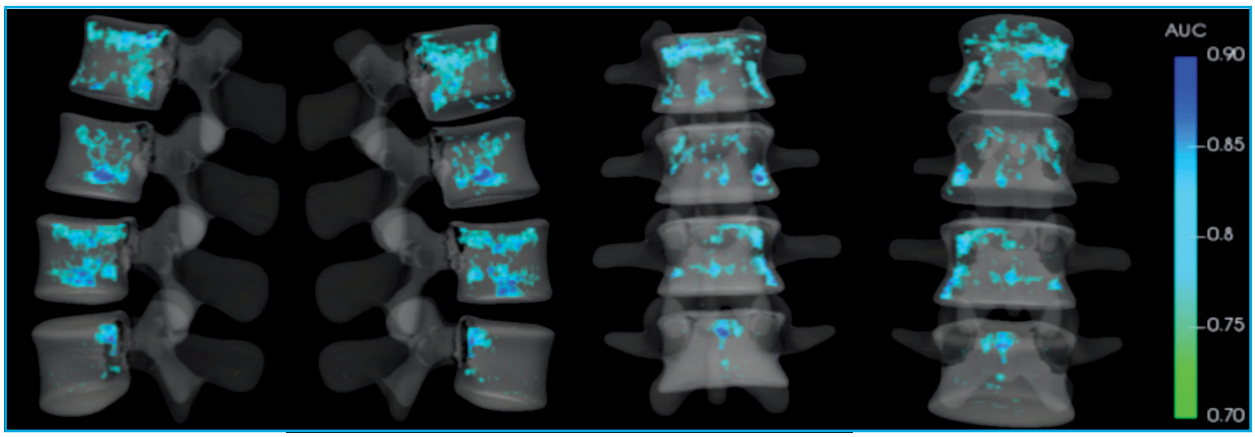

Figure 3. Top: anatomical distribution of the mean differences in the cortical sBMD of the vertebral body between the subjects included in the experimental group and the control group. Non-significant changes (unpaired Student t-test) are shown in grey. Bottom: AUC was calculated by using the cortical sBMD at each vertex of the vertebral body surface of the subjects included in the experimental group and the control group. The regions where the differences in the cortical sBMD were not significant (unpaired Student t-test), in the region of interest of the total vertebra, are shown in grey. The regions listed at an AUC greater than the 90th percentile (that is, an AUC>0.777) are circled in red. The maximum AUC was 0.836

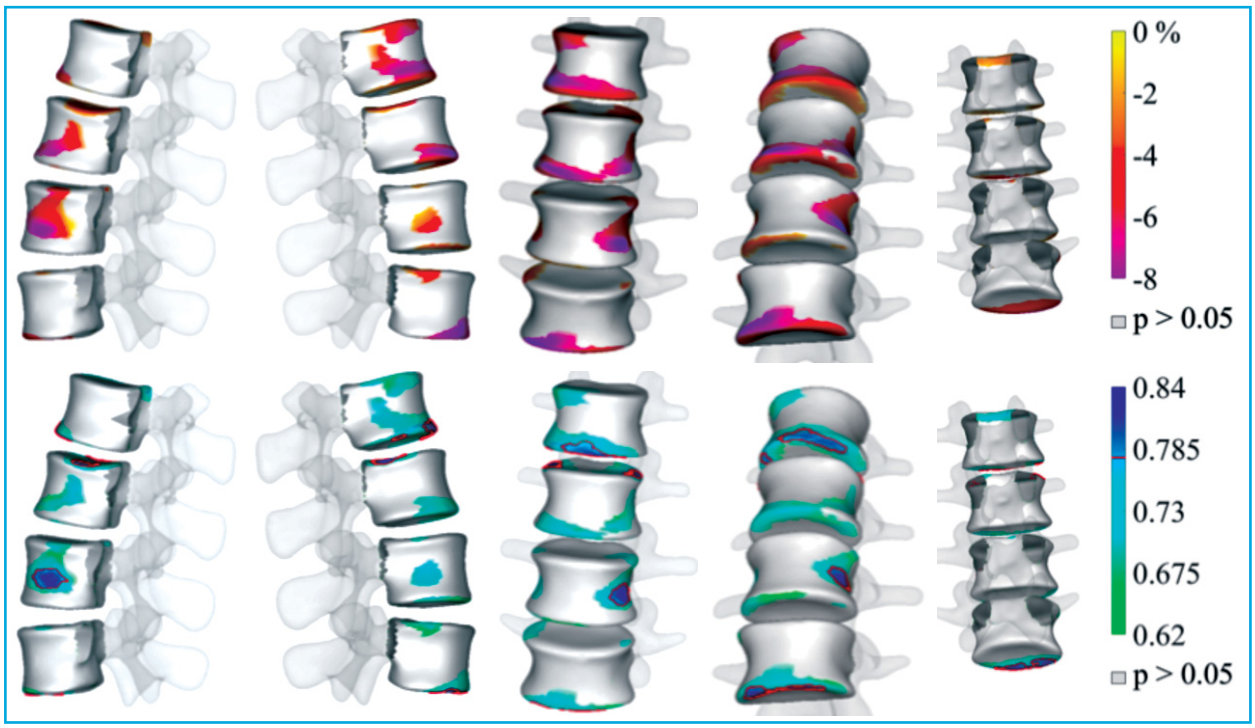

bral body (OR=4.557; 95% CI: 1.411-14.718 in the integral bone, and OR=5.060; 95% CI: 1.406-18.208 in the trabecular bone) in comparison with the aBMD (OR=1.862; 95% CI: 0.862-4.022). These results are consistent with various studies present in the literature, where it was found that the OR for QCT-derived measurements of vBMD are similar or higher, if compared with aBMD measurements[14,16]. Melton et al.[14] reported a slightly higher OR for vBMD in the L1-L3 segment (OR=2.2; 95% CI: 1.1-4.3) in the integral bone and OR=1.9; 95% CI: 1.0-3.6 in the trabecular bone), compared to aBMD (OR=0.7; 95% CI: 0.4-1.2). Anderson et al.[15] reported a higher OR for vBMD in L3 (OR=5.3; 95% CI: 1.3-21 in the integral bone and OR=5.6; 95% CI: 1.3-23.4 in the trabecular bone), compared to aBMD (OR=2.8; 95% CI: 1.0-8.0). Grampp et al.[16] reported a higher OR for vBMD in the L1-L4 segment (OR=3.0; 95% CI: 1.5-6.1 in the integral bone and OR=4.3; 95% CI: 1.8-10.1 in the trabecular bone), compared to aBMD (OR=2.4; 95% CI: 1.4-4.2).

The trabecular vBMD in the vertebral body was the measure that best discriminated between the experimental and the control groups, with an AUC of 0.801, compared to 0.662 for aBMD. Similar findings have been found in the literature in studies based on QCT[3,4,11-17,30]. Chalhoub et al.[13] reported an AUC of 0.79 for trabecular vBMD, compared to 0.72 for aBMD. Melton et al.[14] reported an AUC of 0.78 for trabecular vBMD, compared to 0.75 for aBMD. Grampp et al.[16] reported an AUC of 0.82 for trabecular vBMD, compared to 0.78 for aBMD. Imai et al.[20] reported an AUC of 0.77 for trabecular vBMD, compared to 0.71 for aBMD.

Degenerative diseases of the vertebral spine, abdominal aortic calcification, and other sclerotic lesions artificially increase the aBMD measure obtained in the AP DXA[3,4,11,30], despite the fact that patients with such pathologies have a higher risk of fracture. Trabecular vBMD in the vertebral body may be less sensitive to artifacts produced by these diseases, which are often found on the vertebral surface (cortical bone) or in the posterior arch. This could explain the higher AUC values found for the trabecular vBMD in our study. In this sense, 3D measurements derived from the DXA of the trabecular bone in the vertebral body could provide an alternative measure, overcoming the limitation of the diagnosis based on the aBMD by ruling out bone spurs, local deformations in the periosteal surface or in the posterior vertebral processes[30].

In the present study, the differences were less pronounced in the cortical bone (cortical sBMD: -10.1%, AUC=0.734) than in the trabecular bone (trabecular BMD: -16.2%, AUC=0.801). Biomedical studies demonstrated that the contribution of the cortical bone to the vertebral force is usually low in normal subjects, but it could be considerable in subjects with osteoporosis[30,31]. The precision of measurements derived from the DXA in the trabecular and the cortical bones was evaluated in previous works[27]. However, the cortex of the vertebral body is very thin (from 180 to 600 μm with an average thickness of 380 μm)[32], and DXA-based 3D modelling methods can hardly model local deformities, which could affect the precision of the cortical. Cortical sBMD is considered a stronger measure of cortical bone than cortical vBMD, since generally it is easier to measure in low-resolution images[31,32].

Local differences between the experimental and the control groups were analyzed using color-coded images. The mean differences in the trabecular vBMD between the subjects included in the experimental groups and those in the control group and their respective AUC were greater near the end plates and smaller in the centre of the vertebral body. Experimental studies of vertebral fractures in specimens show how the end plates of the vertebral body are the regions where failure at a tissue level begins[33-36]. These findings are consistent with biomechanical studies that show that the maximum load fraction on the trabecular bone normally occurs near the end plates[20,35,36]. The anatomical distribution of mean differences in cortical sBMD between subjects included in the thoracic spine fracture subgroup and their respective subjects in the control subgroup shows more pronounced differences in the end plates[33-36]. The results are consistent with biomechanical studies showing the thickness and density of the end plate, and the density of the adjacent trabecular bone as good predictors of local stiffness and strength.

The most significant limitation of the present study is the small number of subjects included. The main difficulties in including subjects in the experimental group were to find patients with DXA images from before the incident fracture, since most patients go to the doctor's office after the fracture event, and to ensure that the subjects did not present prevalent osteoporotic fractures in any bone at the time of the initial baseline visit. Furthermore, our study is monocentric, only includes postmenopausal Caucasian females and not all of them have the same fractured vertebra. Therefore, the results can only be extrapolated to populations with similar characteristics. Besides, due to the design of our study (retrospective and case-control), we cannot directly imply a causal association between the reduction of 3D measurements derived from DXA and osteoporotic fracture. Another limitation is that the participants included in this study did not undergo a QCT examination. Therefore, we were unable to make a direct comparison between the results obtained using 3D measurements derived from DXA and measurements derived from QCT. Nor was a comparison made of 3D measures derived from DXA and other methods used in clinical practice to predict fracture risk (such as the Trabecular Bone Score –TBS– or the FRAX® tool). Furthermore, the presence/absence of vertebral fracture was confirmed by anteroposterior DXA scans and vertebral morphometry (VFA, Vertebral Fracture Assessment). It would have been interesting to include other imaging modalities such as QCT or X-ray to further assess vertebral fractures.

Conclusions

This case-control study showed the association between 3D measurements derived from lumbar DXA and incident osteoporotic fractures in the dorsal vertebrae. The individuals in the experimental group showed lower values of vBMD measured in different vertebral regions and compartments compared to the values measured in the group of control subjects. Trabecular vBMD in the vertebral body was the measure that best discriminated between the experimental and control groups. Methods based on 3D modelling based on DXA could be a valuable option to complement standard 2D measurements derived from DXA in the management of osteoporosis. Similar studies involving larger cohorts will be conducted in future researches to determine whether 3D measurements derived from lumbar DXA could improve the prediction of fracture risk in clinical practice. Case-control studies will also be carried out with subjects presenting exclusively osteopenia according to the aBMD criteria.

Acknowledgments: We would like to thank the support of the Industrial Doctorate program of the Generalitat de Catalunya, as well as the QUAES Foundation - UPF Chair in Computational Tools for Health Purposes. The research that led to these results also received funding from the State Program for Research, Development and Innovation Oriented to the Challenges of Society, Ministry of Economy and Competitiveness (Reference: RTC-2014-2740-1) and from the Eurostars program (project ID: 9 140), financed by the Centre for Industrial and Technological Development, Ministry of Economy and Competitiveness. Furthermore, the author Mirella López Picazo received a FEIOMM grant to present the results of this work at the ASBMR 2018.

Conflict of interests: López Picazo M is an employee of Galgo Medical. Humbert L is a shareholder and employee of Galgo Medical. Di Gregorio S, González Ballester MA and Del Río Barquero LM have no conflicts of interest.

Bibliography

1. Johnell O, Kanis JA. An estimate of the worldwide prevalence and disability associated with osteoporotic fractures. Osteoporos Int. 2006;17:1726-33.
2. Ballane G, Cauley JA, Luckey MM, El-Hajj Fuleihan G. Worldwide prevalence and incidence of osteoporotic vertebral fractures. Osteoporos Int. 2017;28:1531-42.
3. Kanis JA. Diagnosis of osteoporosis and assessment of fracture risk. Lancet. 2002;359:1929-36.
4. Kanis J A, Johansson H, Oden A, McCloskey EV. Assessment of fracture risk. Eur J Radiol. 2009;71:392-7.
5. Marshall D, Wedel H. Meta-analysis of how well measures of bone mineral density predict occurrence of osteoporotic fractures. BMJ. 1996;312:1254-59.
6. Siris ES, Chen YT, Abbott TA, Barrett-Connor E, Miller PD, Wehren LE, et al. Bone mineral density thresholds for pharmacological intervention to prevent fractures. Arch Intern Med. 2004; 164:1108-12.
7. Dimai HP. Use of dual-energy X-ray absorptiometry (DXA) for diagnosis and fracture risk assessment; WHO-criteria, T- and Z-score, and reference databases. Bone. 2017;104:39-43.
8. Gordon CM, Lang TF, Augat P, Genant HK. Image-based assessment of spinal trabecular bone structure from high-resolution CT images. Osteoporos Int. 1998:8:317-25.
9. Genant HK, Wu CY, van Kuijk C, Nevitt MC. Vertebral fracture assessment using a semiquantitative technique. J Bone Miner Res. 1993;8:1137-48.
10. Prevrhal S, Fox JC, Shepherd JA, Genant HK. Accuracy of CT-based thickness measurement of thin structures: Modeling of limited spatial resolution in all three dimensions. Med Phys. 2003;30:1-8.
11. Li N, Li XM, Xu L, Sun WJ, Cheng XG, Tian W. Comparison of QCT and DXA: Osteoporosis detection rates in postmenopausal women. Int J Endocrinol. 2013;2013:895474.
12. Engelke K, Libanati C, Fuerst T, Zysset P, Genant HK. Advanced CT based in vivo methods for the assessment of bone density, structure, and strength. Curr Osteoporos Rep. 2013;11:246-55.
13. Chalhoub D, Orwoll ES, Cawthon PM, Ensrud KE, Boudreau R, Greenspan S, et al. Areal and volumetric bone mineral density and risk of multiple types of fracture in older men. Bone. 2016; 92:100-6.
14. Melton LJ 3rd, Riggs BL, Keaveny TM, Achenbach SJ, Hoffmann PF, Camp JJ, et al. Structural determinants of vertebral fracture risk. J Bone Miner Res. 2007;22:1885-92.
15. Anderson DE, Demissie S, Allaire BT, Bruno AG, Kopperdahl DL, Keaveny TM, et al. The associations between QCT-based vertebral bone measurements and prevalent vertebral fractures depend on the spinal locations of both bone measurement and fracture. Osteoporos Int. 2014;25:559-66.
16. Grampp S, Genant HK, Mathur A, Lang P, Jergas M, Takada M, et al. Comparisons of noninvasive bone mineral measurements in assessing age- related loss, fracture discrimination, and diagnostic classification. J Bone Miner Res. 1997;12:697-711.
17. Kopperdahl DL, Aspelund T, Hoffmann PF, Sigurdsson S, Siggeirsdottir K, Harris TB, et al. Assessment of incident spine and hip fractures in women and men using finite element analysis of CT scans. J Bone Miner Res. 2014;29:570-80.
18. Wang X, Sanyal A, Cawthon PM, Palermo L, Jekir M, Christensen J, et al. Prediction of new clinical vertebral fractures in elderly men using finite element analysis of CT scans. J Bone Miner Res. 2012;27:808-16.
19. Zysset P, Qin L, Lang T, Khosla S, Leslie WD, Shepherd JA, et al. Clinical use of quantitative computed tomography–based finite element analysis of the hip and spine in the management of osteoporosis in adults: the 2015 ISCD Official Positions-Part II. J Clin Densitom. 2015;18:359-92.
20. Imai K, Ohnishi I, Matsumoto T, Yamamoto S, Nakamura K. Assessment of vertebral fracture risk and therapeutic effects of alendronate in postmenopausal women using a quantitative computed tomography-based nonlinear finite element method. Osteoporos Int. 2009;20:801-10.
21. Ahmad O, Ramamurthi K, Wilson KE, Engelke K, Prince RL, Taylor RH. Volumetric DXA (VXA): A new method to extract 3D information from multiple in vivo DXA images. J Bone Miner Res. 2010;25:2744-51.
22. Väänänen SP, Grassi L, Flivik G, Jurvelin JS, Isaksson H. Generation of 3D shape, density, cortical thickness and finite element mesh of proximal femur from a DXA image. Med Image Anal. 2015;24:125-34.
23. Humbert L, Martelli Y, Fonolla R, Steghofer M, Di Gregorio S, Malouf J, et al. 3D-DXA: assessing the femoral shape, the trabecular macrostructure and the cortex in 3D from DXA images. IEEE Trans Med Imaging. 2017;36:27-39.
24. Whitmarsh T, Humbert L, Del Río Barquero LM, Di Gregorio S, Frangi AF. 3D reconstruction of the lumbar vertebrae from anteroposterior and lateral dual-energy X-ray absorptiometry. Med Image Anal. 2013;17:475-87.
25. López Picazo M, Magallon Baro A, Del Rio Barquero LM, Di Gregorio S, Martelli Y, Romera J, et al. 3D subject-specific shape and density estimation of the lumbar spine from a single anteroposterior DXA image including assessment of cortical and trabecular bone. IEEE Trans Med Imaging. 2018;37:1-12.
26. Van der Klift M, De Laet CE, McCloskey EV, Hofman A, Pols HA. The incidence of vertebral fractures in men and women: the Rotterdam Study. J Bone Miner Res. 2002;17:1051-6.
27. Budoff MJ, Hamirani YS, Gao YL, Ismaeel H, Flores FR, Child J, et al. Measurement of thoracic bone mineral density with quantitative CT. Radiology. 2010;257:434-40.
28. López Picazo M, Humbert L, Di Gregorio S, González Ballester MA, del Río Barquero LM. Discrimination of osteoporosis-related vertebral fractures by DXA-derived 3D measurements: a retrospective case-control study. Osteoporos Int. 2019;30:1099-110.
29. Humbert L, Hazrati Marangalou J, Del Río Barquero LM, van Lenthe GH, van Rietbergen B. Technical Note: Cortical thickness and density estimation from clinical CT using a prior thickness-density relationship. Med Phys. 2016; 43:1945-54.
30. Guglielmi G, Floriani I, Torri V, Li J, van Kuijk C, Genant HK, et al. Effect of spinal degenerative changes on volumetric bone mineral density of the central skeleton as measured by quantitative computed tomography. Acta Radiol. 2005;46:269-75.
31. Treece GM, Gee AH. Independent measurement of femoral cortical thickness and cortical bone density using clinical CT. Med Image Anal. 2015;20:249-64.
32. Winzenrieth R, Humbert L, Di Gregorio S, Bonel E, García M, Del Rio L. Effects of osteoporosis drug treatments on cortical and trabecular bone in the femur using DXA-based 3D modeling. Osteoporos Int. 2018;29:2323-33.
33. Noshchenko A, Plaseied A, Patel VV, Burger E, Baldini T, Yun L. Correlation of vertebral strength topography with 3-dimensional computed tomographic structure. Spine (Phila Pa 1976). 2013; 38(4):339-49.
34. Jackman TM, Hussein AI, Adams AM, Makhnejia KK, Morgan EF. Endplate deflection is a defining feature of vertebral fracture and is associated with properties of the underlying trabecular bone. J Orthop Res. 2014;32:880-6.
35. Eswaran SK, Gupta A, Adams MF, Keaveny TM. Cortical and trabecular load sharing in the human vertebral body. J Bone Miner Res. 2006;21:307-14.
36. Jackman TM, Hussein AI, Curtiss C, Fein PM, Camp A, De Barros L, et al. Quantitative, 3D visualization of the initiation and progression of vertebral fractures under compression and anterior flexion. J Bone Miner Metab. 2016;31:777-88.

Rev Osteoporos Metab Miner. 2020;12(2):53-61

Impact of vascular calcification on bone health and mortality in kidney transplant patients

DOI: http://dx.doi.org/10.4321/S1889-836X2020000200004

García Castro R[1], Alonso Montes C[2], Gómez Alonso C[2], Martín Carro B[2], Suárez Hevia MA[3], Fernández Gómez JM[3], Suárez Fernández ML[4], Cannata Andía JB[2], Fernández Martín JL[2], Rodríguez García M[4]

1 Nephrology Service. Juaneda Miramar Hospital. Juaneda Assistance Network. Palma de Mallorca (Spain)
2 Bone and Mineral Reseach Unit. Central University Hospital of Asturias (HUCA). Institute of Health Research of the Principality of Asturias (ISPA). Kidney Research Network - Carlos III Health Institute (REDinREN-ISCIII). Oviedo University. Oviedo (Spain)
3 Clinical Management Area Urology. Central University Hospital of Asturias. Oviedo (Spain)
4 Clinical Management Area Nephrology. Central University Hospital of Asturias. Oviedo (Spain)

Date of receipt: 17/03/2020 - Date of acceptance: 08/04/2020

Summary

Objetive: To assess the prevalence of vascular calcification and vertebral fractures in a cohort of patients undergoing kidney transplantation and its association with all graft-related causes of mortality and dysfunction, as well as the relationship with biochemical parameters of bone and mineral metabolism.

Material and methods: Prospective, observational, single-center study, which included 405 patients undergoing kidney transplants, with collection of clinical, biochemical, epidemiological parameters, and of radiological vascular calcification and vertebral fractures by simple radiography at the time of transplantation, with a minimum follow-up of two years. We assessed cardiovascular mortality and all causes and decreased glomerular filtration. In addition, 39 bone densitometry studies carried out in the months prior to transplantation were reported.

Results: Patient survival was significantly lower in the group of patients with vascular calcification (131±1.5 months without calcification compared to 110±3.5 months with vascular calcification, p<0.001). A greater decrease in the estimated glomerular filtration rate (GFR) was observed using the CKD-EPI formula in all patients who presented vascular calcification, this being an independent risk factor (OR=2.7; 95% CI: 1.6-4 , 4; p<0.001). The prevalence of vertebral fractures was significantly higher in the vascular calcification group (12%), independently of other risk factors (OR=9.2; 95% CI: 1.2-73.4; p=0.036). The prevalence of vertebral fractures has been associated with lower hip bone mass assessed by bone densitometry (T-score -1.2 vs. -2.4, p=0.02)

Conclusions: Vascular calcification prior to transplantation, evaluated using a simple, cheap and accessible method such as plain radiography, determines the morbidity and mortality of the patient undergoing a kidney transplant and has a great impact on the evolution of graft function, regardless of other risk factors. traditional. The association between bone fragility, vascular calcification and the prognosis of the patient and the renal graft should make us think about adding bone densitometry to the protocol for inclusion in the transplant waiting list. It is relevant to promote not only the best possible vascular health but also to promote the least impact on bone tissue in the progression of chronic kidney disease before the time of transplantation.

Key words: vascular, calcification vertebral fracture, plain radiography, densitometry, kidney transplant, mortality.

Introduction

Chronic Kidney Disease-Mineral and Bone Disorder (CKD-MBD), was defined in 2009 as a set of systemic disorders of the bone and mineral metabolism due to chronic kidney disease, resulting in a combination of the following manifestations[1,2]:

I) Abnormalities of the metabolism of calcium, phosphorus, paratohormone or vitamin D.

II) Anomalies of bone remodeling, mineralization, volume, linear growth or resistance.

III) Vascular and other soft tissue calcifications.

This recently updated definition[3], and the consensus documents of various scientific societies[4], have highlighted the importance of the role of vascular calcification in the morbidity and mortality of patients with chronic kidney disease.

Correspondence: Raúl García Castro (rgccandanedo@gmail.com)

Kidney transplantation is the treatment of choice in renal replacement therapy for patients with CKD, since it improves life expectancy and its quality. However, the impact of recovery of renal function after surgery on alterations in bone mineral metabolism is controversial[5]. Vascular calcifications do not revert after transplantation, and coexist with other alterations of bone-mineral metabolism in the framework of immunosuppressive treatment. The variety of methods used in the detection of vascular calcifications in the studies prior to kidney transplantation, as well as the heterogeneity of the studies available so far, do not allow us to accurately analyze the magnitude of the impact of calcification on the evolution of the renal graft[6].

Loss of bone mass after kidney transplantation occurs mainly in the first 6 months post transplant and decreases as the cortico-steroid dose is reduced[7]. The decrease is 5.5-19.5% during the first 6 months, 2-8% between 6 and 12 months, and 1-2% thereafter. The rapid bone loss that occurs after transplantation conditions high prevalences (7-20%) and incidences (3-4%/year) of fractures, much higher than in the general population as well as in the hemodialysis population[8].

Our main objective was to assess the prevalence of vascular calcification and vertebral fractures in a cohort of patients undergoing kidney transplantation, and its association with graft dysfunction and cardiovascular and all other causes of mortality, as well as the role of loss of bone mass and other alterations of bone and mineral metabolism in the post-transplant evolution.

Material and methods

A prospective, single-center, observational study was designed, which included the 405 patients who underwent kidney transplants between 2008 and 2017, after signing informed consent. Recipients who did not consent to participate in the study and those whose follow-up was less than two years or was carried out in another region, as well as patients with intra-operative surgical complications that forced immediate removal of the graft or who died in the immediate postoperative period were excluded (n=95). The study was approved by the Research Ethics Committee of the Principality of Asturias.

A systematic collection of clinical, biochemical, and epidemiological parameters at the time of transplant and a follow-up after the intervention of at least two years were carried out in all included patients. The following were collected:

1. General and anthropometric data: age at the time of the transplant, sex, height, weight, body mass index.

2. Data on kidney disease and renal replacement therapy (RRT) prior to transplantation: cause of CKD, residual diuresis, time on dialysis, modality of RRT.

3. Cardiovascular risk factors and clinical history: hypertension (HT), diabetes mellitus (DM), dyslipidemia (DL), tobacco use.

4. Average biochemical data of the 6 months prior to transplantation: serum calcium (Ca), serum phosphorus (P), serum hemoglobin (Hb), paratohormone (PTH) and albumin (Alb).

5. Data on kidney transplantation: data were collected on the age of the donors, the rate of non-functioning kidney graft, the rate of initial graft dysfunction (those patients who needed to continue dialysis during the first days after surgery), the rate of acute immune rejection, and HLA (human leukocyte antigen) compatibility.

6. Radiological evaluation of vascular calcifications and vertebral fractures in pre-transplant studies: the radiological study consisted of carrying out radiographs of the anteroposterior pelvis, dorsal spine, and lumbosacral in anteroposterior and lateral views.

Radiological studies were blindly evaluated by two independent experts. The agreement between the same observer and interobserver[9] was evaluated, with a kappa index of 0.74, in both cases (for the presence of aortic vascular calcification, and the presence or absence of vertebral fractures, without considering the severity of the calcifications or the type/degree of fractures).

Vascular calcifications were defined as any calcification of the region of the abdominal aorta, iliac, femoral, uterine/spermatic arteries (more than two isolated patchy calcifications or a visible linear calcification in a section of the vessel)[10]. For the analysis of mortality and cardiovascular events, calcification of the abdominal aorta has been used as it is the most prevalent in the study cohort.

The semi-quantitative classification of Genant[11] has been used to establish the existence of osteoporotic vertebral fracture in the dorsal and antero-posterior and lateral lumbosacral radiological images, as long as they presented wedging, bi-concavity and/or crushing grade 1 of Genant or higher.

7. Evaluation by CKD-MBD densitometry: bone mineral density (BMD) was measured in the posteroanterior lumbar spine (L2-L4) and in the right femoral neck, using a DXA Hologic® QDR-1000 densitometer (Hologic Inc., Waltham, Massachusetts. USA). There were 39 studies available in the two years before transplantation.

8. Assessment of kidney function and bone metabolism of the transplant patient: creatinine, estimated glomerular filtration rate (GFR) according to the CKD-EPI formula (Chronic Kidney Disease Epidemiology Collaboration), Ca, P, PTH in intervals of 3, 6, 12 and 24 months. Mortality from all causes was evaluated, with a mean follow-up time of 7.2±2.4 years (minimum of 2 years, maximum of eleven years), as well as mortality from cardiovascular events (acute myocardial infarction, AMI, and/or cerebrovascular accident, CVA), and graft dysfunction not justified by immunological cause[12]. This is understood as a marked decrease in glomerular filtration rate in the post-transplant follow-up.

Statistic analysis

The descriptive analysis is shown as percentages (%), means (X) and standard deviations (SD), or medians (Mn) and interquartile range in the variables that did not have a normal distribution.

For the analysis of the differences between the clinical and biochemical parameters, and their association with vascular calcification, statistical T-Student tests, Chi-square test, multiple logistic regression analysis and non-parametric tests were used (U-Mann Whitney) when necessary, with a 95% confidence interval (CI), and considering a value of $p<0.05$ as statistically significant.

For survival analysis, Kaplan Meier curves were calculated, along with multivariate logistic regression and Cox regression analysis. Statistical analysis was carried out using IBM® SPSS® Statistics v.20.00 for Windows software.

Results

Table 1 shows the general characteristics of the patients included in the study. Regarding the biochemical parameters related to bone mineral metabolism in the six months prior to transplant, the mean serum calcium value was 9.17±0.85 mg/dl, serum phosphorus 4.45±1.31 mg/dl, albumin 38.3±4.4 mg/dl, hemoglobin 11.3±1.9 g/dl and the median of PTH of 244 pg/ml, with an interquartile range between 150 and 360.

The donors' mean age was 54±12 years, with a correlation with the age of the recipients of R=0.645 (p<0.001), the never functioning graft rate was 3.5%, the percentage of initial dysfunction of the graft with subsequent recovery was 35.5%, the acute rejection rate was 11%, and the mean HLA compatibility was 2±1.

In the analyzed areas, 66.4% of the study patients presented some type of radiological vascular calcification, with no differences between the different dialysis modalities. Thus, 64.2% had calcification at the abdominal aorta level, 53% had calcification at the iliac level, 40.6% had calcification in the femoral region and 23.9% had calcification in the uterine or spermatic arteries, although reference here will only be made to calcification in the abdominal aorta. The baseline characteristics of the patients and the parameters of the CKD-MBD, according to the existence or not of previous radiological vascular calcification, are shown in table 2.

Table 1. General characteristics of the patients included in the study

	N=310
Age (years), X ± DE	55 ± 12
Sex (man), %	61.6
Height (cm), X ± DE	166 ± 9
Average weight (kg), X ± DE	74 ± 15
BMI (kg/m^2), X ± DE	26.68 ± 4.84
CKD etiology, %	
Glomerulonephritis	24.5
HPD	18.4
Idiopathic	15.5
Mellitus diabetes	13.4
Arterial hypertension	11.6
Others	6.1
Modality TRS, %	
HD	56.5
PD	35.8
CKD	7.7
Dialysis T (months), Mn [Rn]	15 [8-31]
HT (Yes), %	86.1
HD (Yes), %	21.3
DL (Yes), %	39
Active smoking (Yes), %	21.3

N: study population; X: mean; SD: standard deviation; BMI: body mass index; CKD: chronic kidney disease; HPD: hepatorenal polycystic disease; HD: hemodialysis; PD: peritoneal dialysis; CKD: advanced kidney disease; T: time; Mn: median; Rn: range; HT: arterial hypertension; DM: diabetes mellitus; DL: dyslipidemia.

The overall prevalence of vertebral fractures in the pretransplant studies was 8.4%; regarding bone densitometry studies (n=39), the values of bone mass in the spine were 0.915±0.176 g/cm^2, with an average T-score of -1.3±1.6, and of 0.717±0.131 g/cm^2 in the hip, with an average T-score of -1.3±1.1, significantly lower in patients with radiological vascular calcification (1.1±1.1 vs. -0.6±0.9; p=0.045). The results and characteristics of the patients, based on the previous detection or not of vertebral fractures, as well as the result of the available bone densitometries (n=39), are shown in table 3.

A strong association has been found between vascular calcification and vertebral fractures (present in 95% of patients with vascular calcification), and in turn with bone densitometry values, as shown in figure 1. The results of the analysis of logistic regression of risk factors for vascular calcification are shown in table 4.

The evolution of the biochemical parameters of bone mineral metabolism and renal graft function in the post-transplant follow-up is shown in figure 2. A lower GFR was observed in all the patients who had calcification, and by analyzing the decrease in GFR among the 3 and 24 month follow-up, an average reduction of 3.36 ml/min in patients with vascular calcification in some territory, compared to an increase of 7.31 ml/min in patients without vascular calcification. The results of the multivariate Cox regression analysis, to evaluate the risk factors for the decrease of the GFR in the post-transplant follow-up, are shown in table 4.

The overall mortality rate from all causes was 13.8%, of which 35% were of cardiovascular etiology, 25.8% from infectious complications, 16.1% from neoplastic etiology, and the rest from other causes. Patient survival was significantly lower in the group of patients with vascular calcification (131±1.5 months without calcification compared to 110±3.5 months with vascular calcification, p<0.001), as shown in the Kaplan-Meier analysis in figure 3. Analyzing the mortality of cardiovascular etiology exclusively (ischemic stroke or acute myocardial infarction), the findings were identical (Log Rank=7.43, p<0.001), without any patient without previous vascular calcification presenting a fatal cardiovascular event. The independent risk factors for mortality, according to the multivariate Cox regression analysis, both cardiovascular and for all causes, are shown in table 5, where the results of the bone densitometry studies were not included, given their small number. The vertebral BMD was 0.902±0.172 g/cm^2 in the non-deceased patients (n=37) compared to 1,114±0.096 g/cm^2 in the deceased (n=2) (T-score -1.5 vs. 0.6), and the BMD at the hip level was 0.721±0.134 g/cm^2 in the non-deceased compared to 0.678±0.044 g/cm^2 in the deceased (T-score -1.4 vs. -2), with no statistical difference between groups.

Discussion

Cardiovascular mortality is the main cause of death in kidney transplant patients, with an annual risk of lethal or non-lethal events 3 to 5% higher than in the general population. Death with a functioning renal graft accounts for up to 42% of graft losses, with cardiovascular being the most frequent cause, with a prevalence of between 36 and 55%[13] according to the series (in our series, 35%).

Table 2. Baseline characteristics, existence of vertebral fractures and transplant data of the patients based on the existence of radiological vascular calcification in any territory prior to the transplant

	No VC (N=104)	Yes VC (N=206)	p
General and anthropometric data			
Age (years), X ± SD >60 years, %	**48 ± 13 17.9**	**58 ± 10 42.8**	**<0.001****
Sex (man), %	**48.7**	**64.2**	**0.01***
BMI (kg/m^2), X ± SD	25.52 ± 5.93	26.98 ± 4.36	NS**
Kidney disease and replacement therapy facts			
Modality RRT: HD, %	51.3	62	NS *
Modality RRT: PD, %	48.6	37	NS*
Dialysis T >12 months, %	**53**	**66**	**0.04***
Residual diuresis (ml), X	731	635	NS**
Cardiovascular risk factors and clinical history			
DM (Yes), %	**12.8**	**31.1**	**<0.001***
HT (Yes), %	83.3	87.7	NS*
DL (Yes), %	**25.9**	**45.7**	**<0.001***
Smoking (Yes), %	**19.2**	**33.1**	**0.018***
Biochemical parameters of CKD-MBD in the 6 months prior to transplantation			
Ca (mg/dl), X ± SD	9.21 ± 0.97	9.14 ± 0.78	NS**
P (mg/dl), X ± SD	4.23 ± 1.21	4.57 ± 1.35	NS**
PTH (pg/ml), X ± SD	253 ± 221	299 ± 208	NS**
Alb (mg/dl), X ± SD	38.5 ± 4.7	38.25 ± 4.3	NS**
Hb (g/dl), X ± SD	11.4 ± 1.2	11.4 ± 1.1	NS**
Kidney transplant facts			
Donor age (years), X ± SD <50 years, %	**51 ± 12 78.2**	**56 ± 12 59.1**	**0.001****
Graft not functioning, %	2.5	5.1	NS*
Initial dysfunction (Yes), %	**24.3**	**41.5**	**0.007***
Acute rejection (Yes), %	8.9	9.7	NS*
>2 HLA compatible, %	32	27.9	NS*
Radiological evaluation of vertebral fractures and BMD			
Fractures (Yes), %	**1**	**12**	**0,002***
Vertebral BMD (g/cm^2), X ± SD	0.929 ± 0.191	0.905 ± 0.171	NS**
Vertebral T-score, X ± SD	-1.2 ± 1.7	-1.4 ± 1.6	NS**
Hip BMD (g/cm^2), X ± SD	0.751 ± 0.126	0.694 ± 0.132	NS**
Hip T-score, X ± SD	**-1.1 ± 1.1**	**-1.6 ± 0.9**	**0.045****

N: number of patients; X: mean; SD: standard deviation; BMI: body mass index; RRT: renal replacement therapy; HD: hemodialysis; PD: peritoneal dialysis; T: time; DM: diabetes mellitus; HT: arterial hypertension; DL: dyslipidemia; Hb Ca: calcium; P: serum phosphorus; PTH: paratohormone; Alb: albumin; Hb: hemoglobin; BMD: bone densitometry; NS: not significant; *: Chi squared; **: T Student.

The role of bone mineral metabolism associated disorders with CKD in the morbidity and mortality of kidney transplantation has already been described by other authors[8,14]. One of the main manifestations of CKD-MBD is vascular calcification. There are numerous methods for detecting calcification and multiple scales to quantify it. Cianciolo et al.[6], in their 2014 meta-analysis, included up to 13 calcification studies in kidney transplant recipient patients, evaluating different territories and using different diagnostic techniques. In most of these studies, a progression of calcification was observed in the post-transplant in all the territories, depending on their initial severity[15].

The presence of vertebral fractures also has a negative impact on the prognosis of CKD patients, being an independent mortality factor in CKD patients in stages 3-5, and has been associated with the existence of vascular calcifications in patients on hemodialysis[10], and in studies in the general population[16]. These findings are identical to those of our series, where the existence of previous vertebral fractures increased the risk of vascular calcification by nine times.

Table 3. Vertebral fractures and clinical characteristics of the patients

	No fractures (N=284)	Yes fractures (N=26)	p
General and anthropometric data			
Age >60 years, %	32.7	47.6	NS*
Sex (woman), %	40.3	47.7	NS*
IMC (kg/m^2), X ± SD	26.73 ± 4.9	27.31 ± 2.98	NS**
Kidney disease and replacement therapy facts			
Dialysis T (months), Mn [Rn]	17 [9-33]	26 [11-32]	NS***
Cardiovascular risk factors and clinical history			
DM (Yes), %	27%	9%	NS*
Smoking (Yes), %	27.4%	19%	NS*
Biochemical parameters of CKD-MBD in the 6 months prior to transplantation			
VC (Yes), %	**63.9**	**95**	**0.01***
Ca (mg/dl), X ± SD	9.1 ± 0.9	9.3 ± 0.6	NS**
P (mg/dl), X ± SD	**4.5 ± 1.3**	**3.9 ± 1.1**	**0.04****
PTH (pg/ml), X [Rn]	250 [155-365]	130 [96-385]	NS***
Alb (mg/dl), X ± SD	**38.16 ± 4.5**	**40.34 ± 2.98**	**0.03****
Hb (g/dl), X ± SD	11.4 ± 1.2	11.5 ± 1.1	NS**
Radiological evaluation of vascular calcifications and BMD			
VC (Yes), %	**63.9**	**95**	**0.01***
Vertebral BMD (g/cm^2), X ± SD	0.927 ± 0.172	0.847 ± 0.204	NS**
Vertebral T-score , X ± SD	-1.2 ± 1.6	-2.1 ± 1.7	NS**
Hip BMD (g/cm^2), X ± SD	**0.739 ± 0.121**	**0.599 ± 0.137**	**0.01****
Hip T-score, X ± SD	**-1.2 ± 0.9**	**-2.4 ± 1.2**	**0.02****

N: number of patients; X: mean; SD: standard deviation; BMI: body mass index; T: time; Mn: median; Rn: interquartile range; DM: mellitus diabetes; VC: vascular calcification; Ca: calcium; P: serum phosphorus; PTH: paratohormone; Alb: albumin; Hb: hemoglobin; BMD: bone densitometry; NS: not significant; *: Chi squared; **: T Student; ***: U Mann-Whitney.

However, given the absence of acute symptoms or the existence of back pain from multiple causes, the existence of fractures is rarely investigated in daily clinical practice. A prevalence of vertebral fracture between 8 and 45% has been demonstrated in patients undergoing kidney transplantation when bone deformities were investigated[17] (in our series, 8.4% in the six months prior to transplantation). Until the recent update of the KDIGO guidelines (Kidney Disease: Improving Global Outcomes)[3], BMD was not systematically recommended, so in our series we present a limited number of studies. Despite this, we found a lower T-score in the femoral neck of patients with vascular calcification and in turn associated with the existence of previous vertebral fractures. Considering bone mass in the femoral neck a better marker of vertebral fractures than the lumbar bone mass falls within expectations, given the possibility of radiological image artifacts, among others, due to aortic calcification itself[18]. Furthermore, there are PTH levels in patients before transplantation, leading to greater involvement in a predominantly cortical bone location, such as the femoral neck, compared to predominantly trabecular areas, such as the lumbar spine. Our results also concur with a recent study that determines BMD's importance as a predictor of fractures in renal patients[19], although carrying out densitometric studies with a greater number of patients that allow us to ratify our findings is required.

Among the biochemical parameters, attention is drawn to significantly higher albumin values among fractured patients, indicating that these patients' bone fragility would not be conditioned by greater nutritional deterioration[20,21].

Simple radiology provides the lowest dose of radiation possible, allows joint evaluation of vascular calcification and fractures, and has proven useful as a predictor of mortality in dialysis patients. Rodríguez et al.[10], in a study of 193 hemodialysis patients who underwent a plain radiograph of the lumbar spine and pelvis, demonstrated an increase in the prevalence of calcification in the aorta of patients with chronic kidney disease on hemodialysis, and associated its severity with time on dialysis, with vertebral fractures and with morbidity and mortality.

In our series, the overall prevalence of vascular calcification at the time of transplantation was 66.4%, coinciding with the findings of previous series[10,22]. As expected, the existence of radiological vascular calcification has been associated with diabetes mellitus prior to transplantation, sex, time on dialysis of more than 12 months, active smoking, the existence of vertebral fractures and, above all, from of the sixth decade. These findings are similar to others already published, even in the general population[6,10,16]. No significant differences were found regarding the existence of calcification between the modalities of renal replacement therapy, and there were also no diffe-

Figure 1. Vascular calcification, vertebral fractures and hip bone densitometry in patients undergoing kidney transplantation

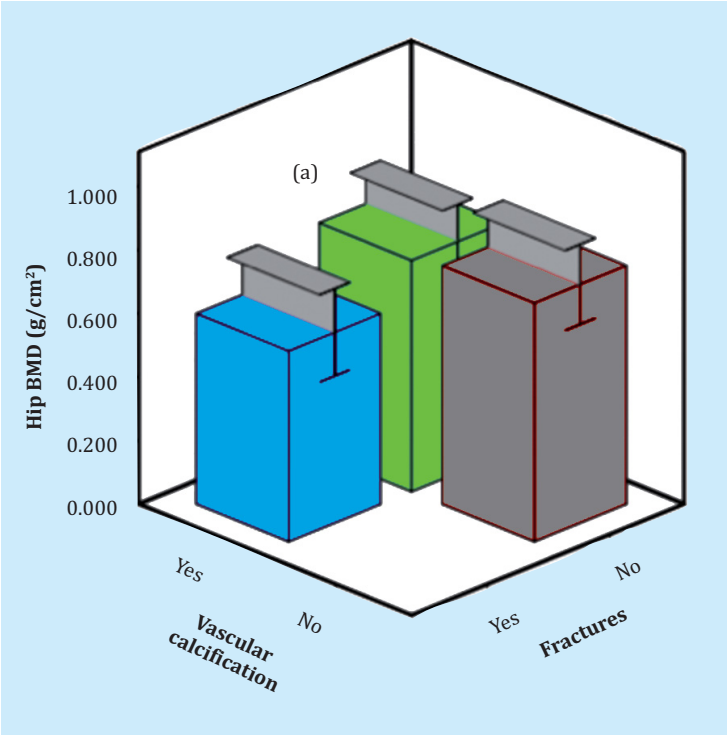

(a): the mean hip bone mass values for different categories of vascular calcification (bars) and the standard deviation of these values are shown in the figures; cm^2: square centimeter; BMD: bone densitometry; g: gram.

Figure 2. Evolution of biochemical parameters and graft function

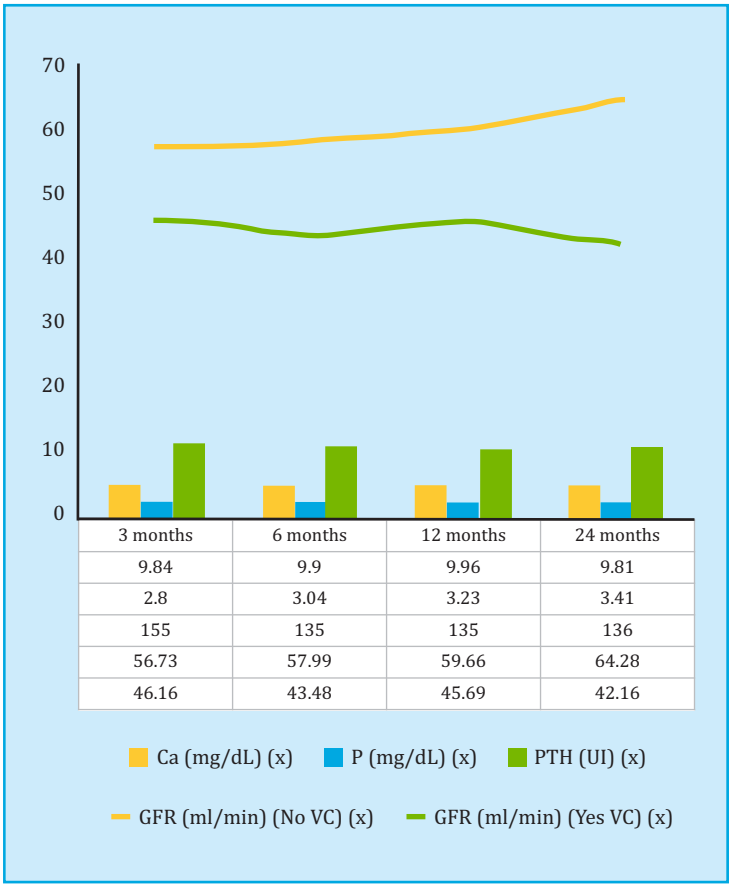

3 months	6 months	12 months	24 months
9.84	9.9	9.96	9.81
2.8	3.04	3.23	3.41
155	135	135	136
56.73	57.99	59.66	64.28
46.16	43.48	45.69	42.16

rences regarding the values of calcium, phosphorus and serum PTH in the 6 months prior to transplant, similar to some studies. published[23] where no differences are found regarding vascular calcification association, although there is controversy among various authors[24].

Regarding the renal graft, the age of the donors was higher in patients with vascular calcification, and it was correlated with the age of the recipients (R=0.65; p<0.001), with higher rates of initial graft dysfunction. (41.5% vs. 24.3%); This finding is related to the selection of older donors for older patients, in accordance with the protocols of the different scientific societies that recommend that organs removed from patients of a certain age be transplanted in patients in a range of ± 15 years[25]. In the post-transplant follow-up, a higher rate of decrease in the GFR was observed in the group of patients with calcification; Although this could only be attributed to the age of the donors (lower in patients without calcification), the Cox regression analysis showed vascular calcification in any territory as an independent risk factor (OR=2.8; p<0.001). Other factors, such as the initial graft dysfunction, which could be understood as predisposing for a worse posterior evolution, did not show statistical significance.

No association was found between the decrease in GFR and the rest of the biochemical parameters of bone mineral metabolism evaluated at follow-up, as in other recent studies, such as that of Wolf et al.[14], where only FGF-23 showed an impact in the evolution of long-term filtering (not included in our analysis). In the immediate post-transplant, hypercalcemia has been described as one of the main factors of graft dysfunction in the medium term, due to the appearance of tubular microcalcifications[26]. In our analysis, the calcaemia did not show an impact on the decrease in the filtrate. In future studies, it would be interesting to analyze the impact of other biomarkers, such as α-klotho, on post-transplant follow-up.

The overall survival of the patient undergoing transplantation was greater in patients without previous radiological calcification, as occurs in other previous studies[27], even in the general population[28]. In the multivariate analysis, vascular calcification in the abdominal aorta showed an impact on the mortality of the patients in the post-transplant follow-up, together with the decrease in glomerular filtration, smoking, and advanced age. No association has been found between all-cause mortality and the existence of vertebral fractures, which has been reported by other authors[10,16]. Similarly, survival free of fatal cardiovascular events was greater in patients without vascular calcification. In our cohort, all the patients who died from car-

Table 4. Risk factors assessed

Risk factors for the existence of vascular calcification in any territory (Multiple logistic regression analysis)		
	Odds ratio [a] (CI 95%)	**p**
Age (>60 years), (34.5%)	**4 (1.9-8.5)**	**0.01**
Sex (man), (61.6%)	**2 (1.1-3.8)**	**0.032**
Mellitus diabetes (Yes), (23.3%)	**2.8 (1.2-6.3)**	**0.014**
Dyslipidemia (Yes), (61%)	1.8 (0.9-3.5)	NS
Smoking (Yes), (21.3%)	**2.6 (1.3-5.6)**	**0.01**
Dialysis T (>12 meses), (58.7%)	**2.2 (1.1-4.2)**	**0.017**
Fractures (Yes), (8.4%)	**9.2 (1.2-73.4)**	**0.036**
Risk factors for decreased glomerular filtration rate in the post-transplant follow-up (Cox multivariate regression analysis)		
	Odds ratio [a] (CI 95%)	**p**
Age >60 years (Yes), (34.5%)	1.2 (0.7-1.9)	0.42
Sex (man), (61.6%)	0.9 (0.6-1.4)	0.77
Mellitus diabetes (Yes), (23.3%)	1.1 (0.7-1.6)	0.8
Dyslipidemia (Yes), (39%)	1.1 (0.7-1.6)	0.91
Active smoking (Yes), (21.3%)	1.1 (0.7-1.7)	0.66
Dialysis T (>12 months), (58.7%)	1.4 (0.9-2.2)	0.09
Donor age <50 years, (65.2%)	**0.5 (0.3-0.8)**	**0.008**
Initial dysfunction (Yes), (35.5%)	0.7 (0.5-1.1)	0.09
Vascular calcification (Yes), (66.4%)	**2.7 (1.6-4.4)**	**<0.001**
Previous fractures (Yes), (8.4%)	1.3 (0.7-2.5)	0.45

CI: confidence interval; T: time; NS: not significant; [a]: adjusted for all risk factors included in the table. The percentage of patients in the study cohort that presented this risk factor is shown in parentheses.

diovascular events had some type of vascular calcification in the abdominal aorta, at least moderate, in addition to having suffered one or more vertebral fractures, so we have not been able to analyze its impact on cardiovascular mortality.

The main limitation of this study is that risk factors such as immunosuppressive therapy and infectious complications during follow-up have not been included, as well as the small number of bone densitometry studies available, given the low recommendation for their performance in previous guidelines[2]. It is important to point out the need to include this study in daily clinical practice, as part of the evaluation prior to kidney transplantation, due to its association with vascular calcification, which in turn determines significant morbidity and mortality. Another existing limitation is the absence of regulated vitamin D measurements, since very low values are associated with an increase in the progression of aortic calcification, as well as mortality, even in the general population[29].

Figure 3. Overall survival of the kidney transplant patient based on the existence of radiological vascular calcification

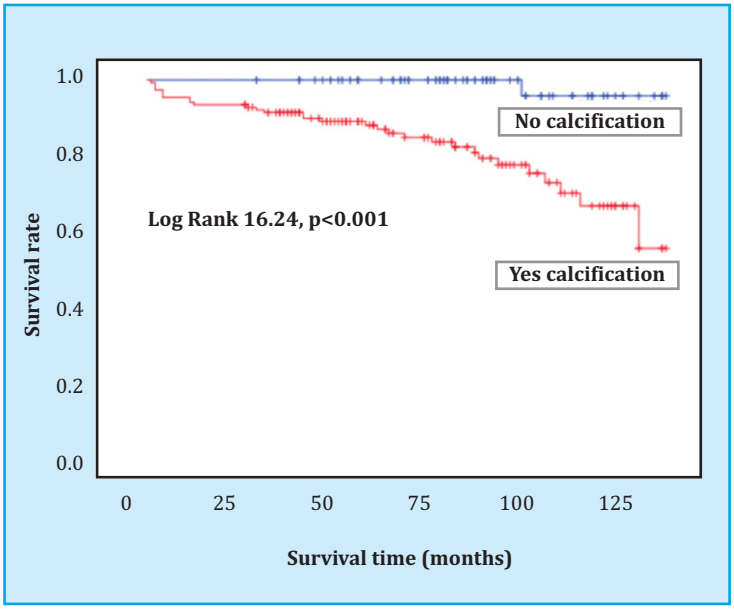

Table 5. Risk factors for all-cause mortality and cardiovascular etiology (Cox multivariate regression analysis)

Mortality	Global (N= 43) [a]		Cardiovascular (N=15) [b]	
	HR [a] (CI 95%)	p	HR [a] (CI 95%)	p
Age (>60 years), (34.5%)	**3.5 (1.4-8.4)**	**0.005**	2.9 (0.7-12.1)	0.12
HT (Yes), (86.1%)	0.7 (0.2-1.9)	0.46	0.5 (0.1-2.5)	0.4
DM (Yes), (23.3%)	1.1 (0.4-2.3)	0.99	1.1 (0.3-4.1)	0.92
Dyslipidemia (Yes), (39%)	0.5 (0.2-1.1)	0.07	0.6 (0.1-2.2)	0.41
Tobacco (Yes), (21.3%)	**4.6 (1.6-12.7)**	**0.003**	**4.8 (1.1-23.5)**	**0.049**
VC AA (Yes), (64.2%)	**8.8 (1.1-69.3)**	**0.04**		
Fractures (Yes), (8.4%)	2.1 (0.5-7.7)	0.27		
↓ GFR (Yes), (50.2%)	**4.1 (1.7-12.7)**	**0.003**	**12.1 (1.5-99.2)**	**0.02**

N: number of patients; HR: hazard ratio; CI: confidence interval; HT: arterial hypertension; DM: diabetes mellitus; VC: vascular calcification; AA: abdominal aorta; ↓ GFR: estimated glomerular filtration rate decrease; [a]: adjusted for all included risk factors. The percentage of patients in the study cohort that presented this risk factor is shown in parentheses; [b]: the calcification variable of the abdominal aorta and vertebral fractures were not included in the analysis because they were positive in 100% of the patients who died of cardiovascular mortality.

The main strength of the study is that it includes the evolution of renal graft function over time, and its direct impact on the patient's morbidity and mortality, which in turn will be directly associated with previous vascular calcification.

Conclusion

The results of our study corroborate that vascular calcification prior to transplantation (also associated with vertebral fractures and loss of bone mass) determines the morbidity and mortality of the patient undergoing kidney transplantation and, furthermore, allows us to see its impact on the evolution of the function of the grafting, regardless of other traditional risk factors. Plain radiography, cheaper and harmless than other procedures, and included in most evaluation protocols prior to kidney transplantation, can therefore give us certain information on the prognosis and evolution of patients, and help prevent potential future complications. It is relevant to promote not only the best possible vascular health, but also the least impact on bone tissue in the progression of CKD before the moment of transplantation. Therefore, although the study does not have a high number of patients with densitometry, it is recommended that it be carried out as a study prior to inclusion on the transplant waiting list, given the association between bone fragility and vascular calcification, and, in turn, with the prognosis of both the patient and the kidney graft.

Acknowledgments: This work has been possible thanks to the financing obtained from the State Plan for R + D + I 2013-2016, Science, Technology and Innovation Plan 2013-2017 and 2018-2022 of the Principality of Asturias (GRUPIN14-028, IDI- 2018-000152) and by the RETIC of the ISCII REDinREN (RD06/0016/1013, RD12/0021/1023 and RD16/0009/0017), European Regional Development Fund (FEDER) and the Carlos III Health Institute (PI11/00667, PI14/00707 and PI17/00384).

Conflict of interests: Authors declare no conflict of interests. The conduct of this study was in accordance with the ethical principles of the Helsinki Declaration on Clinical Studies.

Bibliography

1. Moe S, Drüeke T, Cunningham J, Goodman W, Martin K, Olgaard K, et al. Definition, evaluation, and classification of renal osteodystrophy: a position statement from Kidney Disease: Improving Global Outcomes (KDIGO). Kidney Int. 2006;69:1945-53.
2. Kidney Disease: Improving Global Outcomes (KDIGO) CKD-MBD Work Group. KDIGO clinical practice guideline for the diagnosis, evaluation, prevention, and treatment of chronic kidney disease-mineral and bone disorder (CKD-MBD). Kidney Int. 2009;76 (Supl 113): S1-S130.
3. Kidney Disease: Improving Global Outcomes (KDIGO) CKD-MBD Update Work Group. KDIGO 2017 clinical practice guideline update for the diagnosis, evaluation, prevention, and treatment of chronic kidney disease–mineral and bone disorder (CKD-MBD). Kidney Int Suppl. 2017;7:1-59.
4. Torregrosa JV, Bover J, Cannata-Andía JB, Lorenzo V, De Francisco ALM, Martínez I, et al. Recomendaciones de la Sociedad Española de Nefrología para el manejo de las alteraciones del metabolismo óseo-mineral en los pacientes con enfermedad renal crónica (S.E.N.-M.M.). Nefrologia Sup Ext. 2011;31(1):3-32.
5. D'Marco L, Bellasi A, Mazzaferro S, Raggi P. Vascular calcification, bone and mineral metabolism after kidney transplantation. World J Transplant. 2015;5(4):222-30.
6. Cianciolo G, Capelli I, Angelini ML, Valentini C, Baraldi O, Scolari MP, et al. Importance of vascular calcification in kidney transplant recipients. Am J Nephrol. 2014;39(5):418-26.
7. Bandenburg VM, Politt D, Ketteler M, Fassbender WJ, Heussen N, Westenfeld R, et al. Early rapid loss followed by long-term consolidation characterizes the development of lumbar bone mineral density after kidney transplantation. Transplantation. 2004;77(10):1566-71.
8. Kalantar-Zadeh K, Molnar MZ, Kovesdy CP, Mucsi I, Bunnapradist S. Management of mineral and bone disorder after kidney transplantation. Curr Opin Nephrol Hypertens. 2012;21(49):389-403.
9. Landis JR, Koch GG. The measurement of observer agreement for categorical data. Biometrics. 1977;33(1):159-74.
10. Rodríguez-García M, Gómez-Alonso C, Naves-Díaz M, Díaz-López JB, Díaz-Corte C, Cannata-Andía JB, et al. Vascular calcifications, vertebral fractures and mortality in haemodialysis patients. Nephrol Dial Transplant. 2009;24(1):239-46.
11. Genant HK, Wu CY, van Kuijk C, Nevitt MC. Vertebral fracture assessment using a semiquantitative technique. J Bone Miner Res. 1993;8(9):1137-48.
12. Kidney Disease: Improving Global Outcomes (KDIGO) Transplant Work Group. KDIGO clinical practice guideline for the care of kidney transplant recipients. Am J Trasplant. 2009;9(Suppl 3): S1-S157.
13. Ojo AO, Morales JM, González-Molina M, Steffick DE, Luan FL, Merion RM, et al. Comparison of the long-term outcomes of kidney transplantation: USA versus Spain. Nephrol Dial Transplant. 2013;28(1):213-20.
14. Wolf M, Molnar MZ, Amaral AP, Czira ME, Rudas A, Ujszaszi A, et al. Elevated fibroblast growth factor 23 is a risk factor for kidney transplant loss and mortality. JAm Soc Nephrol. 2011;22 (5):956-66.
15. Maréchal C, Coche E, Goffin E, Dragean A, Schlieper G, Nguyen P, et al. Progression of coronary artery calcification and thoracic aorta calcification in kidney transplant recipients. Am J Kidney Dis. 2012;59(2):258-69.
16. Naves M, Rodríguez-García M, Díaz-López JB, Gómez-Alonso C, Cannata-Andía JB. Progression of vascular calcifications is associated with greater bone loss and increased bone fractures. Osteoporos Int. 2008;19(8):1161-6.
17. Akaberi S, Simonsen O, Lindergård B, Nyberg G. Can DXA predict fractures in renal transplant patients? Am J Transplant. 2008;8(12):2647-51.
18. Watts NB. Fundamentals and pitfalls of bone densitometry using dual-energy X-ray absorptiometry (DXA). Osteoporos Int. 2004;15(11):847-54.
19. Prasad B, Ferguson T, Tangri N, Yong-Ng Chee, Nickolas TL. Association of bone mineral density with fractures across the spectrum of chronic kidney disease: The Regina CKD-MBD study. Can J Kidney Health Dis. 2019;6. 2054358119870539.
20. Gupta A, Upadhyaya S, Cha T, Schwab J, Bono C, Hershman S. Serum albumin levels predict which patients are at increased risk for complications following surgical management of acute osteoporotic vertebral compression fractures. Spine J. 2019;19(11):1796-802.
21. Nakano T, Kuwabara A, Mizuta H, Tanaka K. Contribution of hypoalbuminemia and decreased renal function to the increased mortality after newly diagnosed vertebral fracture in Japanese subjects. Asia Pac J Clin Nutr. 2016;25(3):472-7.
22. Russo D, Palmiero G, De Blasio AP, Balleta MM, Andreucci VE.: Coronary artery calcification in patients with CRF not undergoing dialysis. Am J Kidney Dis. 2004;44(6):1024-30.
23. Jansz TT, van Reekum FE, Özyilmaz A, de Jong PA, Boereboom FTJ, Hoekstra T, et al. Coronary artery calcification in hemodialysis and peritoneal dialysis. Am J Nephrol. 2018;48:369-77.
24. Noordzij M, Korevaar JC, Bos WJ, Boeschoten EW, Dekker FW, Bossuyt PM, Krediet RT: Mineral metabolism and cardiovascular morbidity and mortality risk: peritoneal dialysis patients compared with haemodialysis patients. Nephrol Dial Transplant. 2006; 21:2513-20.
25. Melilli E, Bestard O, Cruzado JM, Navarro-Zorita I, Grinyó JM, Martínez-Castelao A. Trasplante de riñones con criterios expandidos: manejo y resultados a largo plazo. Nefrologia Sup Ext. 2011;2(5):98-104.
26. Egbuna OI, Taylor JG, Bushinsky DA. Elevated calcium phosphate product after renal transplantation is a risk factor for graft failure. Clin Transplant. 2007;21(4):558-66.
27. Hernández D, Rufino M, Bartolomei S, González-Rinne A, Lorenzo V, Cobo M, et al. Clinical impact of preexisting vascular calcifications on mortality after renal transplantation. Kidney Int. 2005;67(5):2015-20.
28. Iribarren C, Sidney S, Stenfeld B, Browner WS. Calcification of the aortic arch. Risk factors and association with coronary heart disease, stroke and peripheral vascular disease. JAMA. 2000;28(21):2810-15.
29. Zittermann A., Schleithoff S.S., Koerfer R. Vitamin D and vascular calcification. Curr Opin Lipidol.2007;18:41-6.

Rev Osteoporos Metab Miner. 2020;12(2):62-70

Relative fragility of osteoporotic femurs assessed with DXA and simulation of finite element falls guided by emergency X-rays

DOI: http://dx.doi.org/10.4321/S1889-836X2020000200005

Ruiz Wills C[1], Tassani S[1], Di Gregorio S[2], Martínez S[3], González Ballester MA[1,4], Humbert L[5], Noailly J[1], Del Río LM[2]

1 Center for New Medical Technologies (BNC MedTech). Pompeu Fabra University (UPF). Barcelona (Spain)
2 Centro de Tecnología Diagnóstica S.A. Mutua de Terrassa. Terrassa (Spain)
3 Rheumatology Service. Mutua de Terrassa. Terrassa (Spain)
4 Catalan Institute for Research and Advanced Studies (ICREA). Barcelona (Spain)
5 Galgo Medical S.L. Barcelona (Spain)

Date of receipt: 23/01/2020 - Date of acceptance: 10/02/2020

Paper submitted with the support of a 2016 FEIOMM Clinical Research Grant

Summary

Objetive: The diagnosis of osteoporosis has been based on the measurement of bone mineral density, although this variable has a limited capacity in discriminating patients with or without fractures. The application of finite element analysis (FE) on computed tomography volumetric images has improved the classification of subjects by up to 90%, although the radiation dose, complexity, and cost do not favor their regular practice. Our objective is to apply FE analysis to three-dimensional models with dual-energy x-ray absorptiometry (3D-DXA), to classify patients who present osteoporotic fracture of the proximal femur and those without fracture.

Material and methods: A cohort of 111 patients with densitometric osteoporosis was selected: 62 with fracture and 49 without it. Subject-specific FE models for impact were used, such as static simulation of lateral fall. Impact simulations allow identifying the critical region in 95% of cases, and the mechanical response to maximum lateral force. An analysis was performed using a discriminative classifier (Support Vector Machine) by fracture type, tissue and gender, using DXA measurements and biomechanical parameters.

Results: The results showed a classification sensitivity of 100%, and a false negative rate of 0% for cases of neck fracture for trabecular bone in women. The variable major main stress (MPS) is identified as the best parameter for the classification.

Conclusion: The results suggest that using 3D-DXA models help in order to better discriminate patients with raised fracture risk.

Key words: bone densitometry, DXA, bone strength, finite elements, X-ray.

Introduction

The increase in the elderly population and the growing concern about the consequences of fractures, together with insufficient rates of detection of situations of bone fragility[1,2], has increased the indication of the assessment of fracture risk in people of both sexes older than 64 years[3]. The dual-energy X-ray absorptiometry (DXA) technique is currently the clinical standard for this type of bone measurement.

Nowadays, when evaluating the risk of fracture, different methods are applied, although the most widely used include the presence of clinical risk factors and the measurement of areal bone mineral density (BMD). Bone measurements are made in the proximal femur and lumbar spine using DXA. However, BMD only allows a limited assessment of the mechanical determinants of bone fracture[4,5].

Correspondence: Luis del Río Barquero (delriobarquero@gmail.com)

Finite element analysis (FE) has been applied to assess bone resistance in volumetric bone models, based on computed tomography (CT) scans, precisely identifying the subject-specific mechanical determinants of fracture. This type of analysis includes the three-dimensional geometry of the bone, the quantity and distribution of bone tissue, and the loads to which the bone is subjected[6]. With this process, the limitations of the BMDa are overcome. CT-based models of FE have been extensively validated *ex vivo*[7-12], and have shown better performance compared to a BMD in predicting proximal femur resistance *in vitro*[6,13]. A significant association between bone fractures and estimated resistance with FE has also been reported in an *in vivo* study[14].

Numerical models have also addressed fracture risk classification in recent years. In this sense, the bone resistance obtained from the analysis by FE is a better classifier than the BMDa[15,16]. Falcinelli et al.[15] studied the effect of the load condition on fracture through bone resistance. In this study, in the analysis of ROC curves (Receiving Operating Characteristic), the area under the curve (AUC), both in position and under multiple load conditions, was higher than the values obtained for the BMDa. Qasim et al.[16] pointed out that bone strength calculated from CT images with FE was a more reliable predictor of fracture than BMDa obtained with DXA. Both studies used logistic regression to classify fractures.

Nishiyama et al.[17] classified 35 cases of women suffering osteoporotic fractures through femur resistance obtained using a FE model based on quantitative CT (QCT), comparing their classification power with the vBMD. The results obtained with the vector support machine technique showed AUC values of 0.79 and 0.94 for trochanter and neck fractures, respectively. Despite the achievement obtained in this type of study, QCT-based FE models are far from becoming routine clinical practice. Recently, DXA-based three-dimensional (3D) FE models allowed discrimination of fracture cases with AUC >0.80 by using the major principal stress (MPS) as a parameter for discrimination, analyzing for bone tissue type, class of fracture and gender.

A possible improvement of the mechanical analysis of the femur fracture encompasses the study of fracture by regions, which allows filtering the most relevant data of the calculation. However, robust criteria are required to correctly estimate high fracture risk areas and optimize analysis. Furthermore, in most published numerical studies, simulation of a lateral fall has focused on a single load vector. In real conditions, the main load vector, origin of the fracture, may have a different orientation from that assumed in the FE models, affecting the distribution of internal loads and, consequently, the most relevant areas of interest. Some authors[18] have already expressed the need for a broader approach in simulating the load component, among the various determining factors of bone fracture. In the only study in which three fall load conditions were simulated[19], differences in the results were evident.

Therefore, our hypothesis was that the analysis of one of the first diagnostic radiographs of the fracture allows us to infer the spatial orientation of the main load, and to identify the weakest structural sector of the proximal femur, by simulating FE fall. Our objective, then, was to verify, in a case-control study of proximal femur fractures, whether the association of biomechanical parameters related to bone resistance derived from DXA-based FE models improves, taking into account the most advanced representations of the loads associated with the fall and the most affected areas of the bone.

Materials and methods

Subjects

The methodology applied in this study and the use of clinical data and medical images were evaluated by the ethics committee of the University Hospital Mutua de Terrasa, receiving their approval in November 2016.

DXA test data from 111 patients of both sexes with indication of bone densitometry were used, which had been explored in the CETIR department at the University Hospital Mutua de Terrassa. All patients presented osteoporosis, according to the WHO classification, (T-score of lumbar spine, neck of the femur or total area of the femur <-2.5). There was no selection in patients with fracture under the criterion of a T-score >-2.5. Of these patients, 62 had recently suffered a fracture in one of the sectors of the proximal third of the femur after a fortuitous fall (group of cases), and 49 patients, with similar characteristics in terms of age, weight, height, and category according to T-score, had no history of previous fracture (control group). Patient data have been described in table 1, considering the type of fracture and gender.

Medical images

• *X-rays*

The images scanned or by intra-PACS (Picture Archiving and Communication System) of the radiographs of the proximal third of the femur, made to confirm the diagnosis of fracture upon admission to the Hospital's Emergency Department, and prior to limb surgery in which the injury was suspected. From the X-rays of the pelvis and upper sector of the femur in anteroposterior and lateral views, those were selected that reliably showed the fracture, its exact location, the number of fragments and its displacement.

Taking into account the presence and location of the alterations, the following classification was established:
a) Alterations in the neck of the femur:
1. Valgus impact on the femoral head.
2. Complete neck fracture without displacement of fragments.
3. Varus displacement of the femoral head.
4. Complete continuity solution between both fragments.
b) Trochanter alterations:
1. Comminuted fracture with detachment of the lesser trochanter; the caudal end of the neck fragment is located within the medullary cavity of the femoral shaft, with a comminuted posterior wall.
2. Comminuted fracture with the lower end of the neck outside the shaft, medial deviation.
3. Trochanteric fracture where the shaft is displaced inward; with an inverse trace to the first type of alteration.

• *DXA*

DXA testing in patients who have suffered a fracture of the upper third of the femur is carried out a few days after suffering the fracture, and after surgical treatment, according to the type of fracture.

A Prodigy Advance DXA densitometer (GE Healthcare, Madison, Wisconsin, USA) was used. This device employs a narrow angle fan beam that produces X-rays at two different low energies using a cerium K filter, with minimal image distortion. All patients were positioned and scanned

taking into account the manufacturer's recommendations. The patients were placed on the DXA examination table in the supine position, with the feet together, and an internal rotation of the leg to be scanned of 25-30º. EnCore V12.3 software was applied in the analysis. The DXA scan was carried out on the opposite femur to the one that had suffered the fracture, following the manufacturer's recommendations and the official positions of the ISCD (The International Society for Clinical Densitometry).

Table 1. Number of patients recruited by group, sex and type of fracture

Sex	Fractures		Controls
	Neck	Trochanter	
Women	26	19	37
Mens	10	7	12
Total	36	26	49

In patients without fracture, exploration was carried out with similar criteria in the lumbar spine and right femur.

· *3D-DXA*

The DXA files of the proximal femur obtained in two-dimensional (2D) posteroanterior projection were reconstructed to 3D using 3D Shaper® software (version 2.6, Galgo Medical, Barcelona, Spain), with which specific 3D models of each subject were obtained, according to the modeling method implemented and described[14]. Briefly, the algorithm uses a 3D statistical model of proximal femur shape and density, constructed from a database of quantitative computed tomography (QCT) scans of Caucasian men and women. The variables calculated from the 3D reconstruction are:

- Volumetric bone mineral density (BMD): mg/cm^3, in trabecular bone, cortical bone and integrated bone.
- Cortical bone thickness in the following regions: femoral neck, trochanter, diaphysis and total area.
- Cortical surface density: variable obtained by multiplying the density of the local cortical bone by the cortical thickness (in mg) at each point on the external cortical surface (in cm^2).

· *Patient-specific FE models*

The creation of the 3D FE models followed the methodology described in previous works[20,21]. In total, 111 models were reconstructed from the DXA scan files. The bone was considered an isotropic elastic element with a poisson factor of 0.3[22]. The volumetric distribution of bone density (BMDv) was obtained for each model, and the bone stiffness for cortical and trabecular bone was calculated using the following empirical relationships[23,24]:

$$E_{cortical} = 10200\ \rho_{ash}^{2.01} \quad [1]$$

$$E_{trabecular} = 0.0057\ \rho_{app}^{1.96} \quad [2]$$

where $E_{cotical}$ and $E_{trabecular}$ are Young's cortical and trabecular modulus (in megapascals, MPa), respectively, ρash is the density of bone ash in g/cm^3, and ρapp is the bulk density in g/cm^3. The last two were calculated with the following expressions[25]:

$$\rho_{ash} = 0.87\ \rho_{QCT}^{\ -0.079} \quad [3]$$

$$\rho_{app} = \frac{\rho_{ash}}{0.6} \quad [4]$$

where ρQCT is the density obtained by the QCT images approximated by the vBMD, in g/cm^3, obtained by the 3D Shaper® software (Galgo Medical).

Simulations

· Fall simulations

Lateral fall simulations were performed for all models. The simulation consisted of the axial movement of the femur and the impact on a solid surface. A maximum constant velocity was applied to the top of the femoral head in the axial direction toward the surface that was fully fixed (Figure 1a). The speed (V_{impact}) was patient specific taking into account the patient's height (h) and the force of gravity (g) according to the equation [5][26].

Among the biomechanical variables, the major principal stress (MPS), which is the maximum absolute value between the maximum and minimum principal stresses, was used to identify critical regions, which can be compared with radiographs taken immediately after the fracture, to validate model predictions.

$$V_{impact} = \sqrt{2 \cdot g} \cdot h_C \quad [5]$$

$$h_C = 0.51h \quad [6]$$

· *Static simulations*

The mechanical response of the femur due to the lateral fall, was assessed by means of static simulations. A maximum fall force (F_{fall}) was applied to the top of the femoral head, the lesser trochanter was restricted in the direction of the force, and the base of the proximal femur was fixed in all directions (Figure 1b). The fall force depends on the weight and height of the patient[27]. The values of maximum principal strain, major principal strain (MPE), strain energy density (SED), maximum principal stress, and major major stress (MPS) were analyzed in the region of interest (ROI) obtained from the drop simulations. for the trochanter and neck areas. All FE calculations were performed with ABAQUS v2018 kit (Dassault Systèmes Simulia Corp., Johnston, Rhode Island. USA). Deformation (strain) is the modification of the dimension in relation to the dimension prior to stress, expressed in unit length. The tension (stress) is the pressure per unit area and is expressed in pascals (Pa). In our case, the magnitude of the results necesitates using megapascals (Mpa).

ROC-AUC analysis

Following the guidelines of the study by Ruiz Wills et al.[21], the discrimination power of six parameters was tested: the BMDv related to the DXA images extrapolated in 3D, and 5 parameters derived from the FE simulations, ie, the maximum principal deformation, the MPE, the SED, the maximum main voltage and the MPS. The analysis considered the groups of patients (cases and controls), type of fracture (neck and trochanter), type of bone (trabecular and cortical) and gender (female and male). The area under the ROC curve was used to quantify the discriminating power of the evaluated parameters. In addition, a 5 and 4 iteration cross validation was applied for the neck fracture and trochanter discriminations, respectively. This technique is used in artificial intelligence instruments to validate the generated models, guaranteeing that the partition between training and test data is inde-

Figure 1. Limiting conditions of the simulations: A) impact simulations, and B) static simulations

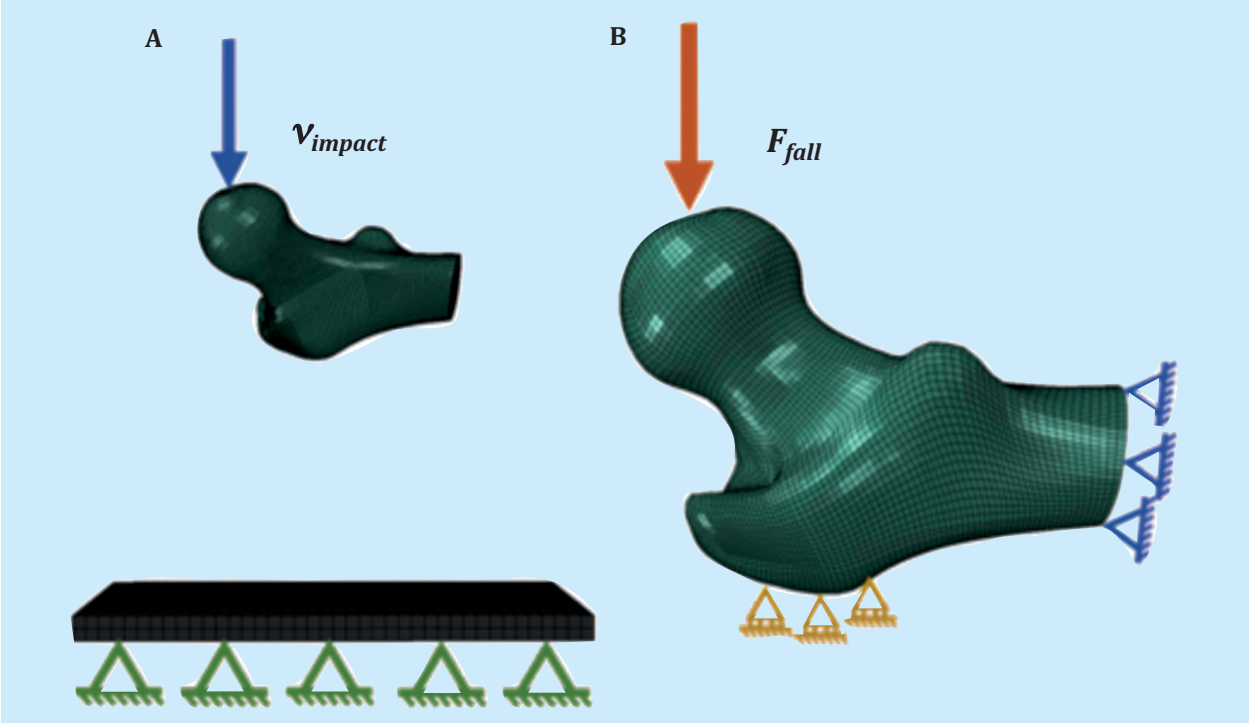

pendent. It consists of repeating and calculating the arithmetic mean obtained from the evaluation measurements on different partitions. The cross validation process is repeated during k iterations, with each of the possible subsets of test data. Finally, the arithmetic mean of the results of each iteration is performed to obtain a single result. This method is very accurate since it is evaluated from K combinations of training and test data.

Classification method

The Support Vector Machines (SVM) were used to classify the fractures. SVM are a set of supervised learning algorithms which solve situations in which an optimal separation between components of a cohort is required, and in which classification and regression problems can occur. The analysis used the same parameters evaluated in the previous section: one related to DXA images and five biomechanical variables obtained from the FE analysis. All parameters were normalized with the mean and the standard deviation:

$$X_{normalized} = \frac{X - \bar{X}}{SD} \quad [7]$$

where X are the values of the parameter to normalize, $\bar{X}$ is the mean of the parameter values for all the elements of the analyzed area, and SD is the corresponding standard deviation.

In addition, the group to which the patients corresponded were considered as the type of fracture. The tissue and sex were selected from the results, where the power of discrimination, obtained in the previous section, was the highest. A 5-iteration cross-validation was included in the analysis. The false negative rate (type II error) was verified as the type of error that should be null or small to consider the analysis to be good.

Results

Region of interest (ROI)

The impact simulation allowed identifying areas in the femur with maximum MPS values. The neck fracture group showed 15,023 elements (geometrically regular fragments into which the bone volume is divided after meshing the finite elements) with high MPS values, while the trochanter group had 42,880 elements (Figure 2). The number of elements identified is 17.9% and 37% lower than the elements used in a previous study carried out in our group for the neck and trochanter, respectively[21]. The area identified for each type of fracture coincided 95% of the time with the fracture line of the available post-fracture X-ray images (Figure 3). As a result, the identified elements were used to carry out the ROC-AUC analysis and classification.

ROC analysis

ROC analysis was carried out regarding the patients' gender. As shown in table 1, the number of men was very small compared to the number of women for both types of fractures. To avoid any misinterpretation of the results, the analysis was applied only to the female population. Table 2 presents the AUC values obtained in the analysis. In trabecular bone, the lowest AUC values were 0.65 for the BMV, and the highest were 0.82 for the MPS, followed by the SED with 0.76, for patients with neck fractures. Trochanteric fracture cases showed similar results, with AUC values of 0.72, 0.82, and 0.83 for BMD, SED, and maximum principal tension, respectively. The maximum AUC value was 0.93 for the MPS. Regarding cortical bone, the BMDv had AUC values of 0.57 and 0.61 for neck and trochanter fractures, respectively. The MPS for trochanter cases provided the highest AUC value: 0.80.

Classification

Based on the results obtained in the previous section, the SVM technique was applied to the data for women, trabecular bone in neck and trochanter fractures. The

confusion matrix for neck fracture showed that the 15 patients without fracture (15/26) were correctly classified, and there was a perfect classification of fracture cases (Figure 4a). For trochanter fractures, 17 (17/23) and 13 (13/15) control and fracture cases were correctly classified, respectively (Figure 4b).

The number of type I errors (false positive, yellow in figure 4) was 11 (11/37) and 2 (2/15) for neck and trochanter fractures, respectively. Furthermore, in trochanteric fractures, 6 cases (6/23) were predicted as a control when, in fact, they fractured: this was a type II error (False negative, red in figure 4).

Equations 8 and 9 represent the linear Kernel equation of the trabecular bone for neck and trochanter fractures, respectively. The values represent the specific weight of each variable in the classification process. The variables SED, maximum main tension and MPS, all presented a greater weight than the BMDv, in cases of neck fracture. Regarding the trochanteric fracture, the MPS variable was the only one that exceeded BMDv. For both types of fractures, the variables related to deformation, that is, the maximum main deformation and the MPE were the least significant of all.

$$M_{neck} = 1.31\ (vBMD) + 0.15\ (Max.\ Prin.\ Strain) + 0.54\ (MPE) + 1.96\ (SED) + 1.80\ (Max.\ Prin.\ Stress) - 2.60\ (MPS) - 1.13 \quad [8]$$

$$M_{trochanter} = 1.33\ (vBMD) - 0.42\ (Max.\ Prin.\ Strain) - 0.38\ (MPE) + 1.17\ (SED) + 0.49\ (Max.\ Prin.\ Stress) + 2.15 - 1.87 \quad [9]$$

Discussion

The impact simulations permitted the identification of critical elements, according to the high MPS values. This result led to refinement of ROI for static simulations (Figure 5). On the one hand, the selection of critical elements such as ROI makes it possible to exclude elements that could contribute noise in the identification of critical stress or deformation concentrations in these areas. On the other hand, refinement of ROI accelerated data extraction and analysis in general.

Consideration of fracture areas is not common in the literature, and when considered, the ROI used is selected according to the anatomical region defined for each type of fracture. As far as we know, this is the first study to use mechanical fields obtained with FE simulations to define ROI for the neck and trochanter areas. This ROI coincides with the fracture lines observed on radiographs taken immediately after the fracture occurred. This result indicates that the impact model is valid for the identification of critical areas for fracture cases. It is relevant to mention that the ROI defined in our study came from the average of all the critical elements of the models for each type of fracture, that is, neck or trochanter.

Figure 2. Area with high values of major main tension (MPS). The blue elements correspond to the element for neck fractures and the red elements are for the trochanter fracture

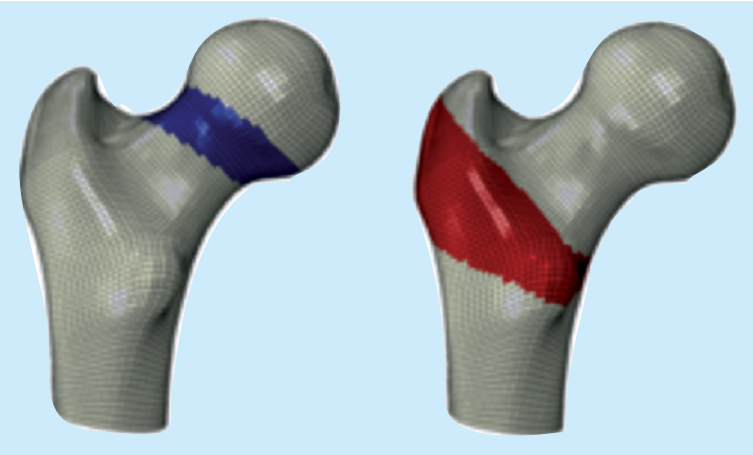

Figure 3. Comparison between the fracture line and the critical area identified for a neck fracture case with high values of major major stress (MPS)

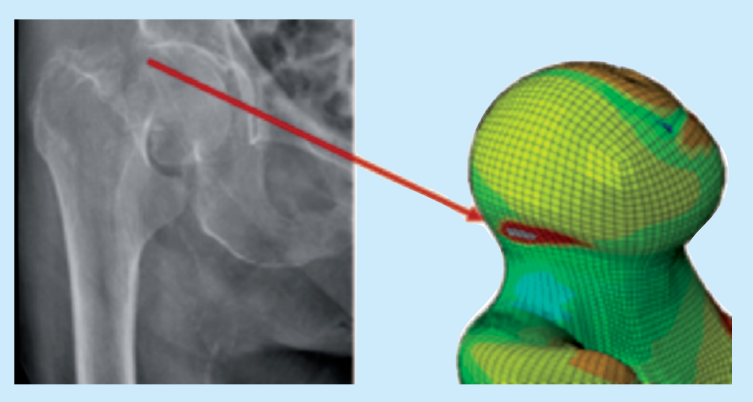

The ROC-AUC analysis for the trabecular bone indicated that the AUC values for the SED, the maximum main tension and the MPS were higher than the values of the BMDv, for both the neck fracture and the trochanter (Table 2). The AUC for MPS increased its discriminating power by 2% (from 0.91 to 0.93) with the new ROI of the trochanter compared to that previously reported in the literature[21]. This increase may be small in absolute terms; however, a 2% increase in AUC values greater than 0.90 is an excellent result. AUC values for cortical bone in the ROI of the trochanter were 0.8, representing an improvement of 13% compared to the values reported in a previous study (0.67)[21]. These results indicate that the selection of the ROI for the analysis has an important influence on the discrimination results. Furthermore, this result confirms that MPS could be the best parameter for fracture classification, as presented in a previous study carried out in our laboratory[21].

Classification analysis was carried out using a VSM only for trabecular bone and women. The results showed a perfect classification, with a sensitivity of 100%, of the cases of femoral neck fracture. Regarding patients without fracture, 58% of cases were classified as true negatives, that is, a specificity of 58%, and the rest of the cases were predicted as fractures. These 11 erroneous classified cases correspond to type I error (false positive), which means that the prediction says that the patient will

Figure 4. Confusion matrix of Support Vector Machine (SVM) for women and trabecular bone: A) neck fracture, and B) trochanter fracture. In green are the true positive cases, in orange the true negatives, in yellow the false positives (type I error) and in red the false negatives (type II error)

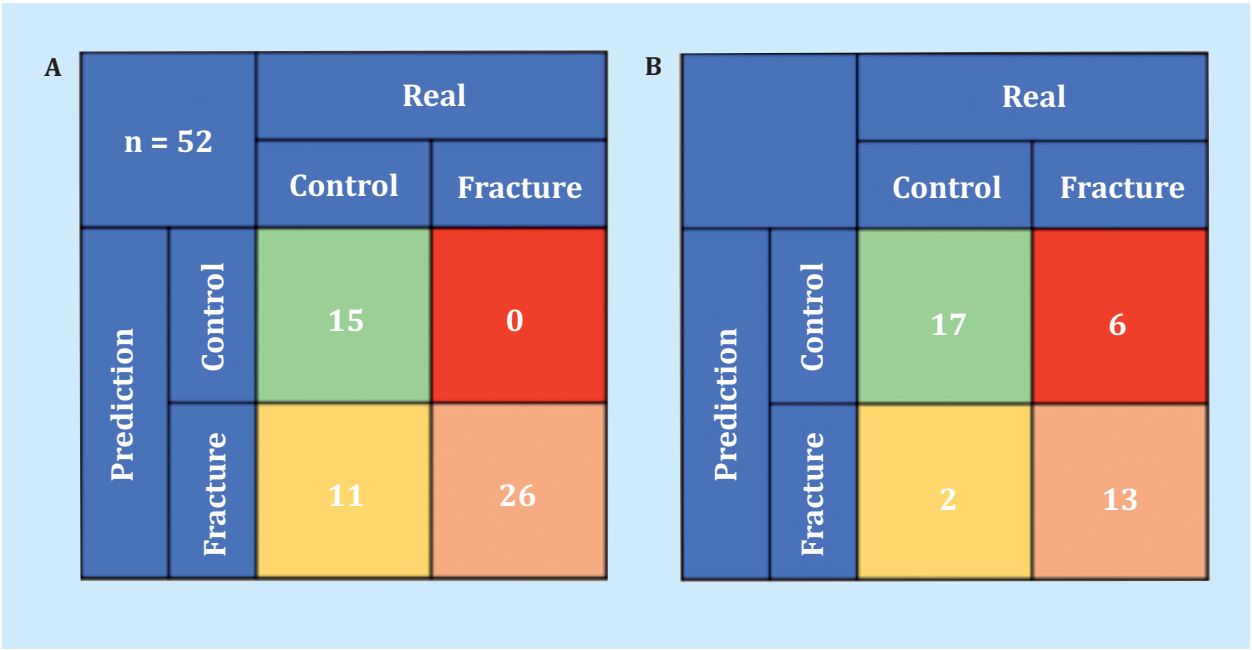

Figure 5. Refinement of the region of interest for: a) neck fracture, and b) trochanter fracture

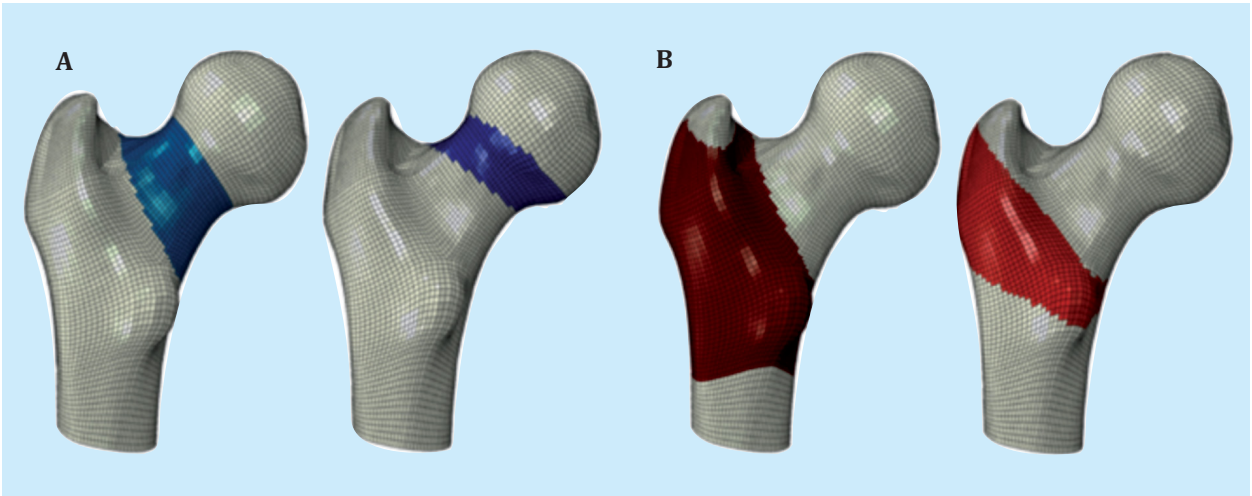

1: proposed fracture analysis zones in Ruiz Wills et al. (2019).
2: real areas.

suffer a fracture when this will not happen or has not yet happened, with the greatest inconvenience of asking the patient to undergo a test or take medicine when it is not necessary. This type of error, in clinical practice, would not be so bad, since steps could be taken to prevent the fracture that may not occur. On the contrary, if the prediction led to a type II error, it would be a worse scenario, since it would indicate that the patient will not suffer any fracture when it really will. No type II error was found for the classification of femoral neck fracture.

For trochanteric fractures, 68% of fracture cases were predicted as a fracture (68% sensitivity), with 6 patients predicted as a control when they fractured, i.e. type II error. A possible explanation could be the definition of ROI for trochanter analysis. Although the ROI was selected based on the critical mechanical fields, the ROI could include some elements that could really affect the results obtained. However, 89% of the control cases were classified as a control (specificity of 89%), and only 2 cases were obtained as a type I error. These results suggest that a larger number of patients may be necessary to extrapolate the results of trochanteric fracture case.

In both cases of fracture, the AUC value for fracture prediction was 0.79. For trochanteric fracture, these values coincide with the values reported in the literature for the same type of fracture[19]. These results suggest that the 3D-DXA-based volumetric femur model may work the same as the QCT-based FE models for the classification of trochanteric fractures. This would be a key point for the use of FE models in routine clinical practice, since DXA exploration can be applied to patients to make the predictive assessment of possible fractures. The AUC for neck fracture

Table 2. AUC values, in the analysis of ROC curves (average cross-validation) for women by ROI and type of bone tissue

Variable	Femur neck		Trochanter	
	Trabecular	Cortical	Trabecular	Cortical
BMDv	0.65	0.57	0.72	0.61
Maximum main deformation	0.65	0.72	0.53	0.65
Major main deformity (MPE)	0.64	0.72	0.55	0.64
Deformation energy density (SED)	0.76	0.73	0.82	0.67
Maximum main voltage	0.82	0.74	0.83	0.74
Higher main voltage (MPS)	0.82	0.74	0.93	0.80

AUC: area under the curve; ROC: receiving operating characteritics; ROI: region of interest.

was lower than that reported in the literature using a model based on the QCT[19]. The AUC value highlights the total number of successfully classified cases, including fractures and controls. However, as previously discussed, there were no type II errors in the classification of neck fracture cases. Overall, these results also indicate that our model can be used to reliably predict neck fractures.

The present study presents certain limitations. The number of men needs to be increased. The extrapolation of the results obtained would be reinforced by the study of a greater number of men. This would provide a better understanding of fracture classification using FE models. Regarding the properties of the bone: the stiffness of the trabecular and cortical bone was calculated using empirical relationships based on BMDv. Macroscopic bone properties can be estimated from the nanoscale bone composition through the theory of homogenization[28-31]. However, the stiffness estimate used in this study is accurate, since the fracture mechanism is outside the scope of our objective[32]. The model used in the drop simulations could only move in the direction of speed. Such a restriction could influence the mechanical response of the bone. However, the impact related to the lateral fall occurs in seconds or a fraction of seconds, and it is highly likely that the damaging force peak will actually occur in the direction of speed, just before impact. As such, restricting all degrees of freedom except in the direction of speed is a reasonable approach. Another point to consider is that the participation of the skin and soft tissues in the impact with the surface has not been taken into account. However, the subject-specific fall force used in the static simulation includes the influence of soft tissues[27]. The subject-specific drop force used in the static simulations was set in one direction. The angle of force has been reported to affect the mechanical response of the bone[33,34]. The angle of application of the force was not modified in this study to simulate the maximum effect that the falling force can have on the mechanical response of the bone. The definition of ROI for neck and trochanter fractures needs to be improved. This study showed that the selection of ROI could influence the results obtained. Automatic subject-specific selection of critical elements can be implemented, by identifying significant differences between the mechanical field obtained from the simulations. This aspect needs to be further explored.

The next step would be to find a strong correlation between the MPS and the parameters derived from the DXA. To achieve this goal, the number of data must be increased to guarantee the accuracy of the correlation found. Once the correlation is established, MPS estimation and hip fracture prediction can be accomplished without the need for any numerical simulation, which can definitely save a lot of time in diagnosis. In this sense, the use of MPS as a fracture classifier/predictor in regular clinical practice may be possible in the near future.

The identification of the MPS variable, with a high predictive value for fragility bone fractures, opens a new stage in obtaining a diagnostic instrument that will potentially allow patients to be identified on the basis of decreased bone strength below of a subject-specific critical level. Inferring the result of this MPS variable from 3D bone measurements is the following objective and its integration with clinical fracture risk factors, not only with the application in femur fractures, but also in the main osteoporotic fractures.

Conclusions

DXA-based 3D FE femur models could be an appropriate tool for classifying patients who may suffer fractures. Defining specific regions of interest for the analysis area would improve the quality of the classification. As such, the definition must be done carefully. Overall, our results suggest that, in clinical practice, FE models of the femur from DXA scans can be used in routine practice to help prevent hip fractures. The number of examinations needs to be increased to define the correlation between MPS and DXA parameters, in order to avoid the use of simulation and accelerate the reliable classification of fracture patients. This point requires continuity in the line of studies and a careful review of the results, modeling a future fracture predictive instrument from DXA explorations with a biomechanical approach, including other well-recognized clinical risk factors.

Funding: This study has been possible with the support of the FEIOMM research grant and financial aid from MINECO (RYC-2015-18888).

Conflict of interests: Authors declare no conflict of interests.

Rev Osteoporos Metab Miner. 2020;12(2):62-70

Bibliography

1. King AB, Fiorentino DM. Medicare payment cuts for osteoporosis testing reduced use despite tests' benefit in reducing fractures. Health Aff (Millwood). 2011;30(12):2362-70.
2. Siris ES, Pasquale MK, Wang Y, Watts NB. Estimating bisphosphonate use and fracture reduction among US women aged 45 years and older, 2001-2008. J Bone Miner Res. 2011; 26(1):3-11.
3. Lewiecki EM, Laster AJ, Miller PD, Bilezikian JP. More bone density testing is needed, not less. J Bone Miner Res. 2012;27(4):739-42.
4. Bouxsein, ML. Determinants of skeletal fragility. Best Pract Res Clin Rheumatol. 2005;19:897-911.
5. Seeman E, Delmas P. Bone quality - the material and structural basis of bone strength and fragility. N Engl J Med. 2006; 354:2250-61.
6. Cody DD, Gross GJ, Hou FJ, Spencer HJ, Goldstein SA, Fyhrie DP. Femoral strength is better predicted by finite element models than QCT and DXA. J Biomech. 1999;32:1013-20.
7. Bessho M, Ohnishi I, Matsuyama J, Matsumoto T, Imai K, Nakamura K. Prediction of strength and strain of the proximal femur by a CT-based finite element method. J Biomech. 2007;40:1745-53.
8. Keyak J, Kaneko T, Tehranzadeh J, Skinner H. Predicting proximal femoral strength using structural engineering models. Clin Orthop Relat Res. 2005;347:219-28.
9. Nishiyama KK, Gilchrist S, Guy P, Cripton P, Boyd SK. Proximal femur bone strength estimated by a computationally fast finite element analysis in a sideways fall configuration. J Biomech. 2013;46:1231-6.
10. Koivumäki J, Thevenot J,Pulkkinen P, Kuhn V,Link TM, Eckstein F, et al. Cortical bone finite element models in the estimation of experimentally measured failure loads in the proximal femur. Bone. 2012;51:737-40.
11. Trabelsi N, Yosibash Z. Patient-specific finite-element analyses of the proximal femur with orthotropic material properties validated by experiments. J Biomech Eng. 2011;133:061001.
12. Schileo E, Taddei F, Cristofolini L, Viceconti M. Subject-specific finite element models implementing a maximum principal strain criterion are able to estimate failure risk and fracture location on human femurs tested in vitro. J Biomech. 2008;41:356-67.
13. Dall'Ara E, Luisier B, Schmidt R, Kainberger F, Zysset P, Pahr D. A nonlinear QCT- based finite element model validation study for the human femur tested in two configurations in vitro. Bone. 2013;52:27-38.
14. Kopperdahl DL, Aspelund T, Hoffmann PF, Sigurdsson S, Siggeirsdottir K, Harris TB, et al. Assessment of incident spine and hip fractures in women and men using finite element analysis of CT scans. J Bone Miner Res. 2014;29 (3):570-80.
15. Falcinelli C, Schileo E, Balistreri L, Baruffaldi F, Bordini B, Viceconti M, et al. Multiple loading conditions analysis can improve the association between finite element bone strength estimates and proximal femur fractures: A preliminary study in elderly women. Bone. 2014;67:71-80.
16. Qasim M, Farinella G, Zhang J, Li X, Yang L, Eastell R, et al. Patient-specific finite element estimated femur strength as a predictor of the risk of hip fracture: the effect of methodological determinants. Osteoporos Int. 2016;27:2815-22.
17. Nishiyama KK, Ito M, Harada A, Boyd SK. Classification of women with and without hip fracture based on quantitative computed tomography and finite element analysis. Osteoporos Int. 2014;25:619-26.
18. Orwoll ES, Marshall LM, Nielson CM, Cummings SR, Lapidus J, Cauley JA, et al. Finite element analysis of the proximal femur and hip fracture risk in older men. J Bone Miner Res. 2009; 24:475-83.
19. Keyak JH, Sigurdsson S, Karlsdottir GS, Oskarsdottir D, Sigmarsdottir A, Kornak J, et al. Effect of finite element model loading condition on fracture risk assessment in men and women: the AGES-Reykjavik study. Bone. 2013; 57:18-29.
20. Humbert L, Martelli Y, Fonolla R, Steghofer M, Di Gregorio S, Malouf J, et al. 3D-DXA: assessing the femoral shape, the trabecular macrostructure and the cortex in 3D from DXA images. IEEE Trans Med Imaging. 2017;36:27-39.
21. Ruiz Wills C, Olivares AL, Tassani S, Ceresa M, Zimmer V, Gonzalez Ballester MA, et al. 3D patient-specific finite element models of the proximal femur based on DXA towards the classification of fracture and non-fracture cases. Bone. 2019;121:89-99.
22. Schileo E, Balistreri L, Grassi L, Cristofolini L, Taddei F. To what extent can linear finite element models of human femora predict failure under stance and fall loading configurations? J Biomech. 2014;47:3531-8.
23. Hodgskinson R, Currey JD. Young's modulus, density and material properties in cancellous bone over a large density range. J Mater Sci Mate. Med. 1992;3:377-81.
24. Keller TS, Carter DR, Hernandez CJ, Beaupre GS. The Influence of Bone Volume Fraction and Ash Fraction on Bone Strength and Modulus. Bone. 2001;29:74-8.
25. Schileo E, Dall'Ara E, Taddei F, Malandrino A, Schotkamp T, Baleani M, et al. An accurate estimation of bone density improves the accuracy of subject-specific finite element models. J Biomech. 2008;41:2483-91.
26. van den Kroonenberg AJ, Hayes WC, McMahon T. Dynamic models for sideways falls from standing height. J Biomech Eng. 1995;117:309-18.
27. Bouxsein ML, Szulc P, Munoz F, Thrall E, Sornay-Rendu E, Delmas PD. Contribution of trochanteric soft tissues to fall force estimates, the factor of risk, and prediction of hip fracture risk. J Bone Miner Res. 2007;22:825-31.
28. Blanchard R, Dejaco A, Bongaers E, Hellmich C. Intravoxel bone micromechanics for microCT-based finite element simulations. J Biomech. 2013;46:2710-21.
29. Fritsch A, Hellmich C, Dormieux L. Ductile sliding between mineral crystals followed by rupture of collagen crosslinks: Experimentally supported micromechanical explanation of bone strength. J Theor Biol. 2009;260:230-52.
30. Morin C, Vass V, Hellmich C. Micromechanics of elastoplastic porous polycrystals: Theory, algorithm, and application to osteonal bone. Int J Plast. 2017;91:238-67.
31. Scheiner S, Pivonka P, Hellmich C. Poromicromechanics reveals that physiological bone strains induce osteocyte-stimulating lacunar pressure. Biomech Model Mechanobiol. 2016; 15:9-28.
32. Yosibash Z, Trabelsi N, Hellmich C. Subject-specific p-FE analysis of the proximal femur utilizing micromechanics-based material properties. Int J Multiscale Comput Eng. 2009;6:483-98.
33. Ali AA, Cristofolini L, Schileo E, Hu H., Taddei F, Kim RH, et al. Specimen-specific modeling of hip fracture pattern and repair. J Biomech. 2014;47:536-43.
34. Grassi L, Schileo E, Taddei F, Zani L, Juszczyk M, Cristofolin, L, et al. Accuracy of finite element predictions in sideways load configurations for the proximal human femur. J Biomech. 2012;45:394-9.

Rev Osteoporos Metab Miner. 2020;12(2):71-76

Postoperative thyroid hypocalcemia diagnosis and management protocol

DOI: http://dx.doi.org/10.4321/S1889-836X2020000200006

Huguet I[1], Muñoz M[2], Cortés M[3], Romero M[4], Varsavsky M[5], Gómez J[6]
1 Endocrinology and Nutrition Service. Infanta Leonor University Hospital. Madrid (Spain)
2 Endocrinology and Nutrition Service. San Cecilio University Hospital. Granada (Spain)
3 Endocrinology and Nutrition Service. Ruber Juan Bravo Hospital. Madrid (Spain)
4 Endocrinology and Nutrition Service. Rafael Méndez General University Hospital. Lorca (Spain)
5 Endocrinology and Nutrition Service. Italian Hospital of Buenos Aires. Buenos Aires (Argentina)
6 General Surgery Service. Ramón y Cajal and Ruber Juan Bravo University Hospital. Madrid (Spain)

Date of receipt: 23/02/2020 - Date of acceptance: 21/06/2020

Summary

Objetive: Transient hypocalcaemia due to hypoparathyroidism is the most frequent complication of cervical surgery (thyroid and parathyroid) and also of reoperations. If mild, hypocalcaemia attributed to hypoparathyroidism is associated with few symptoms or with severe symptoms such as seizures, heart failure, or laryngospasm, in severe cases. Both transient and permanent hypoparathyroidism can have important repercussions on the health of patients. Establishing appropriate protocols are required to prevent, assess and treat these conditions.

Material and methods: A systematic bibliographic search was carried out in Pubmed.gov of available evidence from articles in English and Spanish with inclusion dates until May 2019. Recommendations were made based on the GRADE system (Grading of Recommendations, Assessment, Development and Evaluation).

Results and conclusions: We propose a consensus for patient management of those who are going to undergo thyroid or parathyroid surgery, with different sections for the different stages of the process. This is intended to help clinical decision-making, assist in the discharge process and make referrals to outpatient consultations, thus optimizing resources.

Key words: hypoparathyroidism, hypocalcemia, thyroidectomy.

Introduction

Transient hypocalcaemia due to hypoparathyroidism is the most common complication of cervical surgery (thyroid and parathyroid) and also of reoperations. The deficiency of parathyroid hormone (PTH) secretion causes postoperative hypocalcemia due to an inhibition of bone resorption, a decrease in the synthesis of 1-25-dihydroxy vitamin D by the kidney and reduced intestinal calcium absorption. Some associated comorbidities, such as malabsorption, gastric bypass, and bisphosphonate therapy, may promote parathyroid failure. When PTH secretion is insufficient, hypocalcemia develops. Hypocalcaemia due to hypoparathyroidism is associated with few symptoms, if the hypocalcaemia is mild. In severe cases, symptoms include seizures, heart failure, or laryngospasm. In addition to the magnitude of hypocalcemia, the speed of establishment determines its clinical expression[1].

The removal or inadvertent damage of the parathyroids or the alteration of their blood supply are the responsible causes. Both transient and permanent hypoparathyroidism can have important repercussions on patients' health and establishing appropriate protocols for their prevention, evaluation and treatment are needed[2].

The frequency with which this complication appears is difficult to establish and varies according to the parameters analyzed. These parameters include the definition of hypocalcaemia, its clinical expression and the concept of transient and permanent hypoparathyroidism. A recent meta-analysis of observational studies carried out in the United Kingdom found an incidence after thyroidectomy of 27% (19-38%) for transient hypoparathyroidism, and 1% (0-3%) for permanent hypoparathyroidism[3].

It is important to establish the role of the endocrinologist in the preoperative identification of patients at risk, coordinate management with the surgeon in the immediate postoperative period, and follow-up patients with prolonged hypoparathyroidism.

The aim of our proposal is to develop a protocol for the management of the patient who is going to undergo thyroid or parathyroid surgery, with various sections for the different stages of the process. This helps clinical decision-making and registration process and referral to external consultations, thus optimizing resources.

Correspondence: Isabel Huguet (ihm.huguet@gmail.com)

Clinical definitions

Biochemical hypoparathyroidism: biochemical hypocalcemia accompanied by PTH below the lower limit of the laboratory[1].

Clinical hypoparathyroidism: biochemical hypoparathyroidism accompanied by signs or symptoms of hypocalcaemia.

Parathyroid failure or relative hypoparathyroidism: signs or symptoms of hypoparathyroidism that require medical treatment, despite normal levels[1].

Transient hypoparathyroidism: hypoparathyroidism that recovers in less than 12 months.

Permanent hypoparathyroidism: hypoparathyroidism in need of treatment that lasts over 12 months.

Severe hypocalcaemia: one that presents with symptoms of carpopedal spasm, tetany, seizures, lengthening of the QT interval or hypocalcaemia that, being asymptomatic, presents acutely with corrected calcium levels less than or equal to 7.5 mg/dl, which It could lead to serious complications if left untreated.

Because, in a large part of cases, postoperative hypocalcaemia resolves in the first month after surgery, some authors choose to wait until the 4-6th week to establish the diagnosis of hypoparathyroidism, considering prolonged hypoparathyroidism if there are low PTH levels. or the patient needs treatment from one month after surgery, and permanent when this situation continues beyond one year[2].

Pathophysiology

There a several mechanisms involved in postsurgical hypocalcemia. The most frequent is direct damage to the glands: either due to injury to the vascularization system, mechanical damage, or partial or complete excision of the glands inadvertently or voluntarily. The parathyroid vascularization is complex and its variants make it difficult to carry out surgery. Usually, the inferior thyroid artery is the dominant vessel, supplying both the inferior and superior parathyroids, which also tend to receive a supply from the superior thyroid artery. However, there are individuals with superior thyroid artery dominance or variants in which thyroid thymic anastomoses provide an important component in irrigation[1]. Thus, the surgeon's experience and ability to identify the glands and their vessels are essential in avoiding postoperative complications.

As for the causes of hypocalcemia in the postoperative period, the hungry bone syndrome deserves special mention from the pathophysiologic point of view. This syndrome is classically described in hyperparathyroid patients with significant bone involvement, in which a sudden decrease in PTH levels occurs after parathyroid surgery, leading to sustained hypocalcemia with hypophosphoremia, which may further increase if the remaining parathyroid tissue functions normally. After being chronically hypercalcemic, he is temporarily stunned[4]. Although a classic hungry bone syndrome would not go unnoticed, mild forms of the syndrome are possibly underdiagnosed, so it must be kept in mind at all stages of the surgical process in hyperparathyroid patients, as well as in patients with hyperthyroidism that are going to undergo thyroidectomy and present hypermetabolic bone, either through bone mineral density (BMD) or through bone remodeling markers, such as alkaline phosphatase (AF).

Preoperative assessment

In the patients' preoperative evaluation, we must identify those who are at increased risk of post-surgical hypocalcemia using clinical and biochemical data (Figure 1).

As for the diseases to intervene, patients with hyperthyroidism, with tumors in which lymph node resection is also expected, or patients with simultaneous thyroid and parathyroid surgery, are at higher risk of hypocalcaemia. Likewise, patients with anatomy modified by previous cervical surgery or radiation are at higher risk.

The state of vitamin D should be assessed, since several studies have related its deficit with transient hypocalcemia[3,5-7]. Similarly, it is important to detect patients with malabsorptive problems and request a magnesium determination prior to the intervention.

Once the risk patients have been identified, we suggest treating vitamin D deficiency in patients who are going to undergo thyroidectomy. In the case of parathyroid surgery, although not all studies identify vitamin D deficiency as a key element in the development of postsurgical hypocalcemia[8], given that several studies have shown that correction of vitamin D deficiency does not significantly increase calcaemia[9,10], we suggest, if possible, to treat the deficit at least in patients with higher AF levels or bone involvement.

Recommendations:

- We recommend actively identifying patients with a higher risk of postsurgical hypocalcemia in the preoperative period (1|⨁⨁○○).
- We suggest treating vitamin D deficiency in patients who present increased risk of postoperative hypocalcemia (2|⨁○○○).

Immediate postoperative period

Time after surgery to request initial analysis with PTH

Various groups have studied the usefulness of measuring rapid or intraoperative PTH (PTHiop) and intact PTH (PTHi) in the early postoperative period, which ranges from 10 minutes to 24 hours after thyroidectomy. Depending on its levels, the short half-life of PTH (3-5 minutes) allows decision-making in the postoperative period. PTHiop is determined from blood samples drawn during or shortly after surgery. In many hospitals it provides quick results, while routine determination of intact PTH may not be fast enough to make therapeutic postop decisions[11].

PTHiop levels lower than 7-17.9 pg/ml have been shown to be predictors of hypocalcemia[12-14], as well as postsurgical decreases in PTH greater than 62.5-80%[12,14,15]. Low levels of PTHi, generally <10-15 pg/ml, in the first 24 hours postoperatively, have shown high sensitivity and specificity to predict hypocalcemia development[16-20]. The late decrease in iPTH, equal to or greater than 80%, has demonstrated its utility in selecting patients who are candidates for early hospital discharge[21]. However, the utility of early PTHi levels in predicting permanent hypoparathyroidism is the subject of controversy[22].

The available evidence and the variability of the PTH measurement techniques do not allow us to clearly suggest or recommend the timing of the sample extraction or the cut-off points for deciding early hospital discharge or initiation of treatment for hypocalcaemia.

Initial follow-up of calcaemia and PTH

Assessing calcaemia and PTH in the first 6-8 hours after thyroidectomy and postoperative monitoring of serum

Figure 1. Management in the preoperative phase

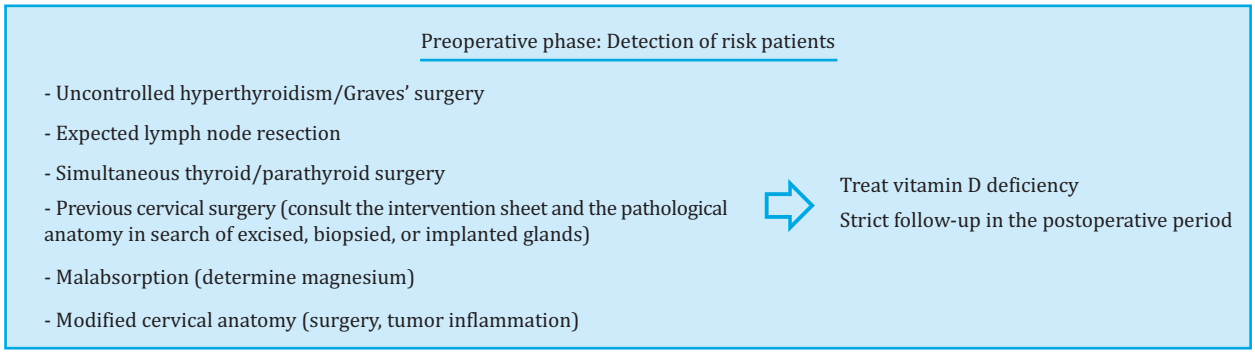

total calcium (albumin corrected) or ionic calcium every 6-12 hours is required to diagnose and monitor postoperative hypoparathyroidism, which will be narrower in the patients at higher risk (Figure 2). The time interval for changes in calcium levels is longer than for PTH, and it may take 24-72 h after surgery for low calcium[11]. Postop calcium levels and variation have been used to establish instructive directions.

Ionic calcium levels (<1-1.1 mmol/l)[23,24] and corrected serum calcium (generally <8 mg/dl)[16,25,26] in the first 24 h postoperatively have been shown to predict hypocalcemic development, although early PTH measurement is more sensitive and cost-effective[25,27]. The joint determination of PTH and calcaemia in the first 24 h postoperative period predicted the development of hypocalcaemia more precisely than each parameter in isolation[16,27]. The variation of total serum calcium in the first postoperative hours has been useful to predict the subsequent evolution: the neutral or positive trend of total calcium (no change or elevation between 2 consecutive postoperative measurements) predicted normocalcemia with a positive predictive value (PPV) 86-100%[28-30]. The negative trend (decrease) in total calcium was associated with the subsequent development of hypocalcemia[28-30].

Since hungry bone syndrome is part of the differential diagnosis of postoperative hypocalcaemia, especially in patients with severe hyperparathyroidism or severe hyperthyroidism with high alkaline phosphatase levels, phosphorus determination may be very useful to differentiate this entity from hypocalcaemia due to hypoparathyroidism, since phosphorus levels will be decreased in the case of rapid remineralization of a bone subjected to hypermetabolism[1,31,32].

If possible, taking turns in Trousseau's sign may be helpful in the postoperative period to identify clinical hypoparathyroidism and relative hypoparathyroidism.

Management of mild-moderate hypocalcemia with oral treatment

The general purpose of treatment is to keep blood glucose lower or slightly below the lower limit of the reference range[1,32,33].

The calcium salt most commonly used for the correction of hypocalcemia is calcium carbonate because it contains more elemental calcium (40%) than calcium citrate (21%). Calcium citrate does not require gastric acidity for its absorption, therefore it can be more useful in patients with achlorhydria, low gastric acidity as observed in patients undergoing treatment with proton pump inhibitors, or patients with gastrectomy. The usual dose is 0.5-2 g of element calcium divided into 2-4 doses. The optimal dose in terms of intestinal absorption seems to be 500 mg of element calcium per dose, since with higher doses a proportional increase in absorption is not achieved. The calcium salt should ideally be taken with meals to guarantee its best absorption and also act as a phosphorus chelator[34-36].

Calcitriol is the active metabolite of vitamin D, which is why it has a rapid onset, increasing calcium absorption at the intestinal level. It is characterized by a shorter half-life (2-3 days) than ergocoleciferol or cholecalciferol (weeks), this being very useful because its effects are more quickly reversible in the case of iatrogenic hypercalcemia. Calcitriol can worsen hyperphosphatemia by increasing absorption of phosphates at the intestinal level. It is administered in doses of 0.25-2.0 µg/day. Occasionally, it is necessary to decrease the intake of phosphates in the diet due to the associated hyperphosphatemia, and phosphate binders can also be administered to decrease hyperphosphatemia in severe cases[35,36].

Treatment of mild and moderate hypoparathyroidism is recommended to be carried out orally (Figure 2). In patients with PTH <15 pg/ml, or decrease in PTH level greater than 75-80% with respect to baseline, serum calcium <8.0 mg/dl or ionic calcium <1.0 mmol/l or <4.0 mg/dl measured within the first 6-8 hours postoperatively, it is recommended to start treatment with elemental calcium 0.5-2 g of element calcium divided into 2-4 doses with meals and calcitriol 0.25-0, 5 µg/day checking calcium and magnesium every 6-12 hours. In case of hypocalcemia progression despite previously described treatment or calcium less than 7.5 mg/dl, calcium should be increased to 1 g every 6 hours and calcitriol to 0.50-1 µg/day divided into twice a day. Also in these cases, intravenous calcium treatment may be necessary. Mild hypocalcemia (Ca >8.0 mg/dl) can be treated with oral calcium supplements[37] in doses of 0.5-2 g of element calcium divided into 2-4 doses.

Since magnesium can decrease in hypocalcemia by inducing a decrease in PTH secretion and resistance to PTH activity, hypomagnesemia, in patients with normal renal function, should be supplemented with magnesium 400-1,000 mg/day, and, Furthermore, reducing constipation associated with high doses of calcium may be useful[34-36].

The administration of calcium salts of levothyroxine should be separated, because it inhibits its absorption. Levothyroxine is recommended to be taken 1 hour before or 3 hours after oral calcium salts[1,31,32].

Recommendations:

- In the first 24 h after thyroidectomy, we suggest determining PTH levels and their percentage decrease

Figure 2. Immediate postoperative management

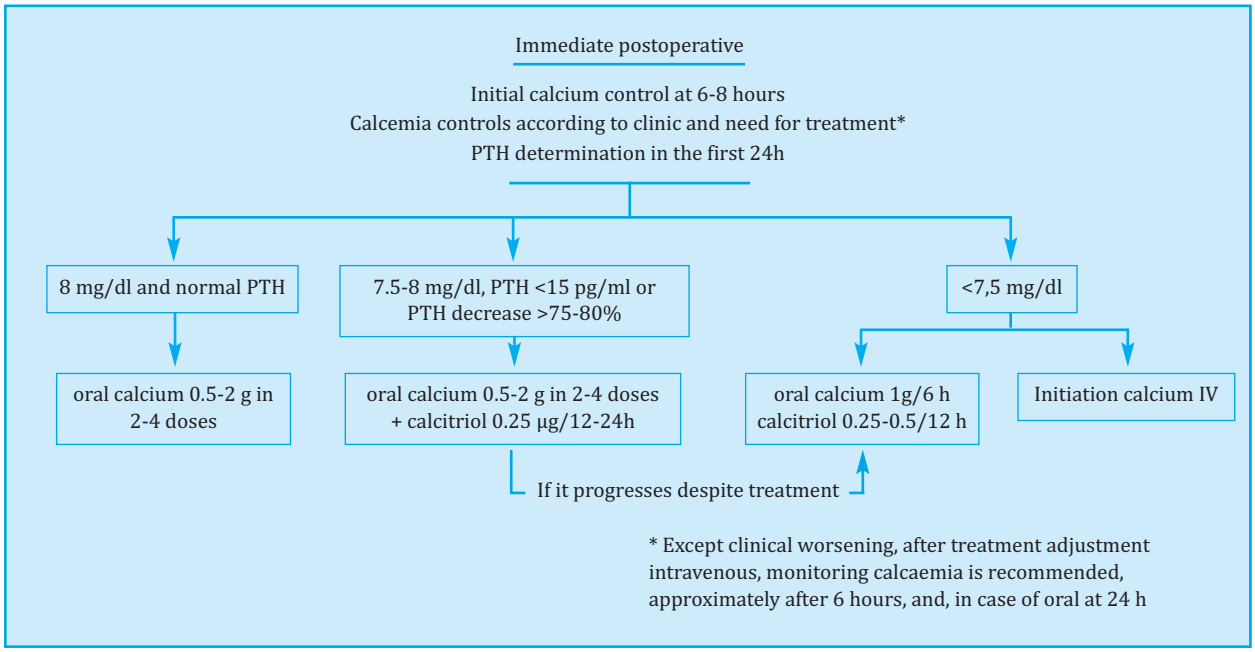

with respect to preoperative values to detect those patients with the highest risk of hypocalcemia (2⊕⊕00).

- The available evidence does not allow us to recommend a specific cut-off point for PTH (absence of recommendation).
- After thyroidectomy, we recommend serial determination of ionic calcium or corrected total calcium to identify those patients with the highest risk of hypocalcemia, candidates for treatment with calcium and/or calcitriol supplements (1|⊕○○○).
- After thyroidectomy, we suggest determination of plasma phosphorus to identify and detect patients with possible hungry bone (2|⊕○○○).
- If possible, we suggest taking the Trousseau sign in turns (2|⊕○○○).
- We recommend orally treating mild and moderate hypoparathyroidism to keep blood glucose lower or slightly below the lower limit of the reference range (1|⊕⊕⊕○).
- We suggest treatment with elemental calcium 0.5-2 g divided into 2-4 doses, with meals and calcitriol 0.25-0.5 mg/day in patients with PTH <15 pg/ml, or decrease in level PTH greater than 75-80% with respect to baseline, or serum calcium <8.0 mg/dl or ionic calcium <1.0 mmol/l (or in mg/dl, ionic <4.0 mg/dl) measured within the first 6-8 h postoperatively, and follow-up with calcium and magnesium controls every 6-12 hours. In the event of hypocalcemia progression despite previously described treatment or calcium less than 7.5 mg/dl, we suggest increasing calcium to 1 g every 6 h and calcitriol to 0.50-1 µg/day divided twice by day and/or intravenous calcium (2|⊕⊕○○).
- We suggest the treatment of mild hypocalcemia (Ca >8.0 mg/dl) with oral calcium supplements in doses of 0.5-2 g in 2-4 doses (2|⊕⊕○○).

Management of severe hypocalcemia

Treatment of severe hypocalcaemia, which presents with symptoms of carpopedal spasm, tetany, seizures or lengthening of the QT interval, or with a level <7.5 mg/dl, even if asymptomatic, is carried out with intravenous calcium.

Initially, treatment will be done with a bolus of 1 or 2 grams of calcium gluconate (GC) in 50 ml of 5% glucose serum or saline infused in 10-20 minutes. This dose raises the calcium level for about two or three hours, so it should be followed by a slow infusion of calcium in patients with persistent hypocalcemia (about 50 mg of element calcium per hour). This is achieved by adding 11 grams of GC = 11 ampoules of 10% GC, with 93 mg of element calcium per ampoule = 1,000 mg of element calcium → in 1,000 ml of 5% glucose serum or saline, to be administered at 50 ml /hour. Patients usually require 0.5 to 1.5 mg of calcium element/kg of body weight/hour. Doses should be adjusted to keep serum calcium below the normal limit[11,36].

Rapid intravenous administration of calcium salts can cause vasodilation, decreased blood pressure, bradycardia, cardiac arrhythmias, syncope, and cardiac arrest. Patients receiving digoxin should be closely monitored for the risk of acute digitalis poisoning due to a probable induction of the positive inotropic action of digoxin. The infusion must not contain bicarbonate or phosphate, as they can form insoluble calcium salts. If these anions need to be perfused, an intravenous line must be used in another limb[38,39]. The use of GC against calcium chloride is recommended, since the latter can cause tissue necrosis if there is extravasation.

The infusion should be maintained until the patient receives an adequate oral calcium and vitamin D regimen that allows target levels to be maintained. For patients with hypoparathyroidism, calcitriol (dose of 0.25 to 0.5 µg twice a day) and oral calcium (3 to 4 grams of element calcium daily, divided into several doses) are recommended, which will be started together with intravenous infusion, stopping the infusion when the calcaemia reaches the lower limit of normality. Regarding treatment with recombinant human PTH (HRTH) in severe hypocalcaemia due to acute hypoparathyroidism, there are very few published data. In an observational study carried out in 8 patients who were administered PTHrh for up to three weeks, a correction of hypocalcaemia was observed in 24

hours[40]. There are also some published cases of the use of HRTH in acute hypoparathyroidism, but without sufficient data to make a recommendation[11,41,42]. The THYPOS phase II study published in 2016 assessed its use in high-risk patients to prevent episodes of acute hypocalcemia and shorten hospital stay, with positive results[43].

Recommendations:

- We suggest the use of intravenous calcium for the treatment of severe hypocalcemia (2|⊕○○○).
- We recommend the use of calcium gluconate versus calcium chloride due to the risk of necrosis in case of extravasation (1|⊕⊕⊕⊕).
- We suggest starting treatment with oral calcium and calcitriol together with intravenous calcium infusion (2|⊕○○○).

Early and late postoperative period

Prophylactic guidelines for calcium and vitamin D supplementation after surgery may delay the recovery of parathyroids after surgical manipulation[44], so we do not recommend their use, which is becoming less and less widespread. In the case of patients who require treatment at discharge, although the strategy of keeping calcium at the lower limit of normality in the first post-surgical month has been used, considering that it could be a stimulus for residual glandular tissue, we are not sure that a hypocalcemic environment is not in itself an attack on the glandular tissue, and further studies are necessary to conclude which level of calcaemia is optimal in the first month after surgery[45]. Patients requiring supplementation at discharge should be reevaluated after 1 or 2 weeks with a new test with determination of calcaemia and PTH, and if calcium levels are normal, treatment will be reduced by approximately half, planning a subsequent reevaluation to try suspend it. It is important that the patient knows the symptoms of hypo and hypercalcemia so that they go to the emergency department if necessary, since discharge is frequent before the plasma calcium nadir is reached[1].

Regarding the management of chronic hypoparathyroidism in the late postoperative period, treatment aims include: keeping the patient asymptomatic; maintain calcium levels close to the lower limit of normal but not exceed 0.5 mg/dl below it; prevent hypocalcemia; achieve a calcium-phosphorus product <55 mg^2/dl^2; and avoid hypercalciuria, hypercalcemia, and ectopic calcifications, including renal[46]. Treatment consists of supplementation with oral calcium and calcitriol and, after the latest guidelines, in which maintaining levels of 25 (OH) vitamin D >20 ng/ml is recommended, supplementing with cholecalciferol or ergocalciferol (the latter not available in Spain) if necessary. The use of thiazides can help control hypercalciuria. Phosphorus chelators may regulate this ion, although its use is only recommended for high levels (>6.5 mg/dl)[36]. Regarding the use of PTH analogues, studies carried out so far have shown that they stabilize plasma levels of calcium and phosphorus, significantly reducing the need for oral treatment. In 2015, the FDA (Foods and Drugs Administration) approved the use of rhPTH (1-84), along with calcium and vitamin D, to treat adults with poorly controlled hypoparathyroidism with conventional therapy, and in 2017 the European Commission did so[47].

Recommendations:

- We suggest a postoperative review 1-2 weeks after discharge with determination of calcaemia and PTH (2|⊕○○○).

Conflict of interests: Authors declare no conflict of interests.

Bibliography

1. Orloff LA, Wiseman SM, Bernet VJ, Fahey TJ 3rd, Shaha AR, Shindo ML, et al. American Thyroid Association statement on postoperative hypoparathyroidism: diagnosis, prevention, and management in adults. Thyroid. 2018;28:830-41.
2. Lorente-Poch L, Sancho JJ, Muñoz-Nova JL, Sánchez-Velázquez P, Sitges-Serra A. Defining the syndromes of parathyroid failure after total thyroidectomy. Gland Surg. 2015;4:82-90.
3. Edafe O, Antakia R, Laskar N, Uttley L, Balasubramanian SP. Systematic review and meta-analysis of predictors of post-thyroidectomy hypocalcaemia. Br J Surg. 2014;101:307-20.
4. Kaya C, Tam AA, Dirikoç A, Kılıçyazgan A, Kılıç M, Türkölmez Ş, et al. Hypocalcemia development in patients operated for primary hyperparathyroidism: Can it be predicted preoperatively? Arch Endocrinol Metab. 2016;60:65-471.
5. Erbil Y, Ozbey NC, Sari S, Unalp HR, Agcaoglu O, Ersoz F, et al. Determinants of postoperative hypocalcemia in vitamin D-deficient Graves' patients after total thyroidectomy. Am J Surg. 2011; 201:685-91.
6. Kirkby-Bott J, Markogiannakis H, Skandarajah A, Cowan M, Fleming B, Palazzo F. Preoperative vitamin D deficiency predicts postoperative hypocalcemia after total thyroidectomy. World J Surg. 2011;35:324-30.
7. Erbil Y, Barbaros U, Temel B, Turkoglu U, Is¸sever H, Bozbora A, et al. The impact of age, vitamin D(3) level, and incidental parathyroidectomy on postoperative hypocalcemia after total or near total thyroidectomy. Am J Surg. 2009;197:439-46.
8. Kaderli RP, Riss P, Dunkler D, Pietschmann P, Selberherr A, Scheuba C, et al. The impact of vitamin D status on hungry bone syndrome after surgery for primary hyperparathyroidism. Eur J Endocrinol. 2018; 178:1-9.
9. Rolighed L, Rejnmark L, Sikjaer T, Heickendorff L, Vestergaard P, Mosekilde L, et al. Vitamin D treatment in primary hyperparathyroidism: a randomized placebo controlled trial. J Clin Endocrinol Metab. 2014;99:1072-80.
10. Grey A, Lucas J, Horne A, Gamble G, Davidson JS, Reid IR. Vitamin D repletion in patients with primary hyperparathyroidism and coexistent vitamin D insufficiency. J Clin Endocrinol Metab. 2005;90:2122-6.
11. Stack BC, Bimston DN, Bodenner DL, Brett EM, Dralle H, Orloff LA, et al. American association of Clinical Endocrinologists and American College of Endocrinology disease state clinical review: postoperative hypoparathyroidismo- definitions and management. Endocr Pract. 2015;21:674-85.
12. McLeod IK, Arciero C, Noordzij JP, Stojadinovic A, Peoples G, Melder PC, et al. The use of rapid parathyroid hormone assay in predicting postoperative hypocalcemia after total or completion thyroidectomy. Thyroid. 2006;16:259-65.
13. Scurry WC, Beus KS, Hollenbeak CS, Stack BC. Perioperative parathyroid hormone assay for diagnosis and management of postthyroidectomy hypocalcemia. Laryngoscope. 2005; 115:1362-6.
14. Alía P, Moreno P, Rigo R, Francos J-M, Navarro M-A. Postresection parathyroid hormone and parathyroid hormone decline accurately predict hypocalcemia after thyroidectomy. Am J Clin Pathol. 2007;127:592-7.
15. Castro A, Del Rio L, Gavilan J. Stratifying the risk of developing clinical hypocalcemia after thyroidectomy with parathyroid hormone. Otolaryngol Head Neck Surg. 2018;158:76-82.
16. Asari R, Passler C, Kaczirek K, Scheuba C, Niederle B. Hypoparathyroidism after total thyroidectomy: a prospective study. Arch Surg. 2008;143:132-7.
17. Youngwirth L, Benavidez J, Sippel R, Chen H. Parathyroid hormone deficiency after total thyroidectomy: incidence and time. J Surg Res. 2010;163:69-71.
18. Kim JP, Park JJ, Son HY, Kim RB, Kim HY, Woo SH. Effectiveness of an i-PTH measurement in predicting post thyroidectomy hypocalcemia: prospective controlled study. Yonsei Med J. 2013;54:637-42.
19. Kala F, Sarici IS, Ulutas KT, Sevim Y, Dogu A, Sarigoz T, et al. Intact parathormone measurement 1 hour after total thyroidectomy as a predictor of symptomatic hypocalcemia. Int J Clin Exp Med. 2015;8:18813-8.
20. Lombardi CP, Raffaelli M, Princi P, Santini S, Boscherini M, De Crea C, et al. Early prediction of postthyroidectomy hypocalcemia by one single iPTH measurement. Surgery. 2004;136:1236-41.
21. Del Río L, Castro A, Bernáldez R, Del Palacio A, Giráldez CV, Lecumberri B, et al. Parathyroid hormone as a predictor of post-thyroidectomy hypocalcemia. Acta Otorrinolaringol Esp. 2011;62:265-73.
22. Lifante J-C, Payet C, Ménégaux F, Sebag F, Kraimps J-L, Peix J-L, et al. Can we consider immediate complications after thyroidectomy as a quality metric of operation? Surgery. 2017;161:156-65.
23. Rosa KM, de Matos LL, Cernea CR, Brandão LG, de Araújo Filho VJF. Postoperative calcium levels as a diagnostic measure for hypoparathyroidism after total thyroidectomy. Arch Endocrinol Metab. 2015;59(5): 428-33.
24. de Andrade Sousa A, Salles JMP, Soares JMA, de Moraes GM, Carvalho JR, Rocha PRS. Course of ionized calcium after thyroidectomy. World J Surg. 2010;34:987-92.
25. Lo CY, Luk JM, Tam SC. Applicability of intraoperative parathyroid hormone assay during thyroidectomy. Ann Surg. 2002; 236:564-9.
26. Lindblom P, Westerdahl J, Bergenfelz A. Low parathyroid hormone levels after thyroid surgery: a feasible predictor of hypocalcemia. Surgery. 2002;131:515-20.
27. Graff AT, Miller FR, Roehm CE, Prihoda TJ. Predicting hypocalcemia after total thyroidectomy: parathyroid hormone level vs. serial calcium levels. Ear Nose Throat J. 2010;89:462-5.
28. Luu Q, Andersen PE, Adams J, Wax MK, Cohen JI. The predictive value of perioperative calcium levels after thyroid/parathyroid surgery. Head Neck. 2002;24:63-7.
29. Güllüoğlu BM, Manukyan MN, Cingi A, Yeğen C, Yalin R, Aktan AO. Early prediction of normocalcemia after thyroid surgery. World J Surg. 2005;29:1288-93.
30. Husein M, Hier MP, Al-Abdulhadi K, Black M. Predicting calcium status post thyroidectomy with early calcium levels. Otolaryngol Head Neck Surg. 2002;127:289-93.
31. Kakava K, Tournis S, Papadakis G, Karelas I, Stampouloglou P, Kassi E, et al. Postsurgical hypoparathyroidism: a systematic review. In Vivo. 2016;30(3):171-9.
32. Kazaure HS, Sosa JA. Surgical Hypoparathyroidism. Endocrinol Metab Clin North Am. 2018;47(4):783-96.
33. Walker Harris V, Jan De Beur S. Postoperative hypoparathyroidism: medical and surgical therapeutic options. Thyroid. 2009; 19:967-73.
34. Gafni RI, Collins MT. Hypoparathyroidism. N Engl J Med. 2019;380(18):1738-47.
35. Tecilazich F, Formenti AM, Frara S, Giubbini R, Giustina A. Treatment of hypoparathyroidism. Best Pract Res Clin Endocrinol Metab. 2018;32:955-64.
36. Brandi ML, Bilezikian JP, Shoback D, Bouillon R, Clarke BL, Thakker RV, et al. Management of hypoparathyroidism: summary statement and guidelines. J Clin Endocrinol Metab. 2016;101:2273-83.
37. Calvo Espino P, Rivera Bautista JÁ, Artés Caselles M, Serrano González J, García Pavía A, García-Oria MJ, et al. Serum levels of intact parathyroid hormone on the first day after total thyroidectomy as predictor of permanent hypoparathyroidism. Endocrinol Diabetes Nutr. 2019;66:195-201.
38. Tohme JF, Bilezikian JP. Diagnosis and treatment of hypocalcemic emergencies. The Endocrinologist. 1996;6:10-8.
39. https://cima.aemps.es/cima/pdfs/es/ft/69465/FT_69465.pdf.
40. Shah M, Bancos I, Thompson GB, Richards ML, Kasperbauer JL, Clarke BL, et al. Teriparatide therapy and reduced postoperative hospitalization for postsurgical hypoparathyroidism. JAMA Otolaryngol Neck Surg. 2015;141(9): 822-7.
41. Mishra PE, Schwartz BL, Sarafoglou K, Hook K, Kim Y, Petryk A. Short-term PTH(1-34) therapy in children to correct severe hypocalcemia and hyperphosphatemia due to hypoparathyroidism: two case studies. Case Rep Endocrinol. 2016;2016:1-4.
42. Andrysiak-Mamos E, Żochowska E, Kaźmierczyk-Puchalska A, Popow M, Kaczmarska-Turek D, Pachucki J, et al. Treatment of severe life threatening hypocalcemia with recombinant human teriparatide in patients with postoperative hypoparathyroidism - a case series. Endokrynol Pol. 2016;67:403-12.
43. Palermo A, Mangiameli G, Tabacco G, Longo F, Pedone C, Briganti SI, et al. PTH(1–34) for the primary prevention of postthyroidectomy hypocalcemia: the THYPOS trial. J Clin Endocrinol Metab. 2016;101:4039-45.
44. Dedivitis RA, Aires FT, Cernea CR. Hypoparathyroidism after thyroidectomy: prevention, assessment and management. Curr Opin Otolaryngol Head Neck Surg. 2017;25:142-6.
45. Sitges-Serra A, Gómez J, Barczynski M, Lorente-Poch L, Iacobone M, Sancho J. A nomogram to predict the likelihood of permanent hypoparathyroidism after total thyroidectomy based on delayed serum calcium and iPTH measurements. Gland Surg. 2017; 6(Suppl 1):S11-9.
46. Bollerslev J, Rejnmark L, Marcocci C, Shoback DM, Sitges-Serra A, van Biesen W, et al. European Society of Endocrinology Clinical Guideline: treatment of chronic hypoparathyroidism in adults. Eur J Endocrinol. 2015;173:G1-20.
47. Mannstadt M, Bilezikian JP, Thakker RV, Hannan FM, Clarke BL, Rejnmark L, et al. Hypoparathyroidism. Nat Rev Dis Primers. 2017;3:17080.


se iomm
Sociedad Española de Investigación Ósea
y del Metabolismo Mineral


fe iomm
Fundación Española de Investigación Ósea
y del Metabolismo Mineral